Chinese Journal of Natural Medicines

Yangxinshi Tablet protects against post-myocardial infarction heart failure with reduced ejection fraction by improving energy metabolism through inhibition of FOXO1/PDK4 signaling

Jingwen Guo, Rong Miao, Qingying Fan, Yilin Li, Yuhua Tian, Aomei Sun, Qingrui Zhang, Zhenguo Lv, Guangwei Qi, Opoku Bonsu Francis, Rui Liu, Ting Chen, Qin Liu, Ruiqiao Li, Jun He, Yan Sun, Ling Leng, Miaomiao Jiang, Qilong Wang

Citation: Jingwen Guo, Rong Miao, Qingying Fan, Yilin Li, Yuhua Tian, Aomei Sun, Qingrui Zhang, Zhenguo Lv, Guangwei Qi, Opoku Bonsu Francis, Rui Liu, Ting Chen, Qin Liu, Ruiqiao Li, Jun He, Yan Sun, Ling Leng, Miaomiao Jiang, Qilong Wang, Yangxinshi Tablet protects against post-myocardial infarction heart failure with reduced ejection fraction by improving energy metabolism through inhibition of FOXO1/PDK4 signaling, Chinese Journal of Natural Medicines, 2026, 24(5), 574-591. doi: 10.1016/S1875-5364(26)61119-3.

View online: https://doi.org/10.1016/S1875-5364(26)61119-3

Wechat

Chinese Journal of Natural Medicines 24 (2026) 574-591

Contents lists available at ScienceDirect

Chinese Journal of Natural Medicines

journal homepage: www.cjnmcpu.com/

Original article

Yangxinshi Tablet protects against post-myocardial infarction heart failure with reduced ejection fraction by improving energy metabolism through inhibition of FOXO1/PDK4 signaling

Jingwen Guo[a], Rong Miao[a], Qingying Fan[b], Yilin Li[a], Yuhua Tian[a], Aomei Sun[a], Qingrui Zhang[a], Zhenguo Lv[a], Guangwei Qi[a], Opoku Bonsu Francis[a], Rui Liu[a], Ting Chen[a], Qin Liu[a], Ruiqiao Li[a], Jun He[a,c,d], Yan Sun[a], Ling Leng[a,c,d,*], Miaomiao Jiang[a,c,d,*], Qilong Wang[a,c,d,*]

[a] *Institute of Traditional Chinese Medicine, Tianjin University of Traditional Chinese Medicine, Tianjin 301617, China*
[b] *Department of Pharmacy, Qingdao Huangdao Peoples Hospital, Shandong 266400, China*
[c] *State Key Laboratory of Component-Based Chinese Medicine, Ministry of Education, Tianjin 301617, China*
[d] *Key Laboratory of Pharmacology of Traditional Chinese Medical Formulae, Ministry of Education, Tianjin 301617, China*

ARTICLE INFO

Article history:
Received 12 August 2025
Revised 21 December 2025
Accepted 1 January 2026
Available online 20 May 2026

Keywords:
Yangxinshi Tablet
Heart failure
FOXO1/PDK4
Energy metabolism
Active ingredients

ABSTRACT

Heart failure (HF) is a major contributor to global morbidity and mortality, with myocardial infarction (MI)-induced HF accounting for a substantial proportion of cases. Although Yangxinshi Tablet (YXS) is clinically used, the mechanisms by which it alleviates HF remain unclear. To elucidate the protective mechanisms of YXS in post-MI HF. An MI-induced HF model was established in male Sprague-Dawley rats, and cardiac function, exercise endurance, hemodynamics, serum biochemical indices, and pathological damage were assessed. To investigate the underlying mechanisms, metabolomics, quantitative polymerase chain reaction (qPCR), ribonucleic acid sequencing (RNA-seq), Western blot, immunofluorescence, chromatin-immunoprecipitation (ChIP)-qPCR, and single-cell RNA-seq were employed. The components of YXS were analyzed *via* molecular docking, and their biological activity was validated in cell-based assays. YXS improved cardiac function and exercise endurance, enhanced hemodynamic parameters, reduced inflammatory cell infiltration, and decreased collagen fiber deposition *in vivo*. *In vitro*, YXS regulated mitochondrial energy metabolism and protected against oxygen-glucose deprivation (OGD)-induced cardiomyocyte injury. Notably, YXS ameliorated post-MI HF by inhibiting forkhead box O1 (FOXO1)/pyruvate dehydrogenase kinase 4 (PDK4) signaling, thereby promoting the tricarboxylic acid (TCA) cycle and increasing adenosine 5'-triphosphate (ATP) levels to restore energy metabolism both *in vivo* and *in vitro*. Senkyunolide H, apigenin, astragaloside IV, and astragaloside VII were identified as active constituents of YXS using an OGD-induced H9c2 cell injury model. These findings indicate that YXS exerts cardioprotective effects in a rat model of post-MI HF. Mechanistically, YXS inhibits FOXO1/PDK4 signaling, enhances TCA cycle activity, and elevates ATP production to improve cardiac energy metabolism and restore energy homeostasis.

1. Introduction

Heart failure (HF) is a clinical syndrome characterized by dyspnea and/or reduced exercise tolerance, resulting from impaired ventricular filling, blood ejection, or both [1]. Globally, the incidence of HF continues to rise, affecting an estimated 23 million individuals, with approximately 50% of cases classified as HF with reduced ejection fraction (HFrEF) [2]. Myocardial infarction (MI), an acute injury to the heart muscle caused by insufficient blood supply [3,4], remains the leading cause of morbidity and mortality worldwide and is the primary contributor to HFrEF [5]. Following an acute MI, the heart frequently undergoes ventricular remodeling, a process that alters both its structure and function. This maladaptive remodeling can lead to cardiac decompensation, manifesting as ventricular dilation and myocardial hypertrophy. The interplay between ventricular remodeling and compromised cardiac function establishes a vicious cycle that ultimately progresses to HF and poses a substantial threat to human health [6]. Although several treatment options are currently available for patients with HFrEF [7-9], the most widely used therapies target the renin-angiotensin system as a cornerstone strategy for HF management [10]. However, numerous studies have reported a strong association between energy metabolism disorders and HF progression [11,12], with traditional Chinese medicine (TCM) formulations such as Qili Qiangxin Capsule and Qishen Yiqi Dripping Pills demonstrating therapeutic potential [13]. Given the pivotal role of energy metabolism dysregulation in HF pathogenesis, further exploration of therapies targeting this mechanism is warranted.

Metabolic disturbances play a crucial role in the development of HF following MI. Under physiological conditions, the

* Corresponding author.
E-mail addresses: lengling@tjutcm.edu.cn (L. Leng); miaomiaojiang@tjutcm.edu.cn (M. Jiang); wangqilong_00@tjutcm.edu.cn (Q. Wang)

https://doi.org/10.1016/S1875-5364(26)61119-3

heart primarily utilizes various metabolic substrates, including fatty acids, glucose, and amino acids, which are funneled into the tricarboxylic acid (TCA) cycle to generate adenosine 5'-triphosphate (ATP) *via* oxidative phosphorylation (OXPHOS) [14]. In HF, however, substrate utilization shifts toward increased glucose consumption relative to fatty acid oxidation [15]. Pyruvate dehydrogenase kinase (PDK) phosphorylates and inhibits pyruvate dehydrogenase (PDH), a key enzyme governing the entry of glucose-derived pyruvate into the TCA cycle, and its activity is sensitive to cellular metabolic status [16]. Forkhead box O (FOXO) transcription factors are critical regulators of energy metabolism [17]. Among them, FOXO1 modulates cell cycle progression and metabolic processes in multiple tissues [18]. In the heart, FOXO1 directly regulates the transcription of PDK4, thereby suppressing PDH activity and acting as a novel upstream regulator of PDK4. Moreover, FOXO1 activation restricts glucose availability for oxidation in cardiomyocytes, contributing to metabolic derangement [19]. During myocardial ischemia, PDK4 overexpression exacerbates cardiomyopathy by promoting metabolic inflexibility and impairing cardiac function, ultimately accelerating the transition to HF [20]. Consequently, targeting energy metabolism regulation has emerged as a promising therapeutic strategy for HF [21].

TCM has a long-standing role in clinical practice, and Chinese herbal formulations are widely used in HF management [22]. Qishen Yiqi Dripping Pills exert anti-fibrotic effects by inhibiting the renin-angiotensin-aldosterone system and reducing levels of collagen I, collagen III, matrix metalloproteinase-2, and matrix metalloproteinase-9 [23]. Qili Qiangxin Capsules significantly attenuate cardiac hypertrophy and improve hemodynamics by activating the adenosine 5'-monophosphate-activated protein kinase (AMPK)/PGC-1α pathway to modulate glucose and lipid metabolism, thereby lowering free fatty acids and lactate to protect cardiomyocytes [24]. TCM operates through a multi-component, multi-target paradigm, and its pharmacological mechanisms in HF treatment have been explored in numerous experimental studies. Yangxinshi Tablet (YXS), a traditional Chinese formulation composed of 13 herbs, has been reported to enhance left ventricular ejection fraction (LVEF), alleviate symptoms, and improve cardiac function in patients with chronic HF [25]. In murine models of ischemia/reperfusion injury, YXS improves cardiac function and exercise tolerance, and it also enhances exercise capacity in healthy mice. Furthermore, YXS has been shown to improve exercise performance in patients with coronary heart disease following percutaneous coronary intervention (PCI) [26, 27]. Beyond its cardioprotective effects *via* energy metabolism regulation, YXS also ameliorates post-PCI mental health issues, demonstrating superior efficacy in reducing depression and anxiety compared to trimetazidine [26]. Mechanistically, YXS activates the PI3K/Akt/mTOR/rpS6/hypoxia-inducible factor-1α (HIF-1α) and AMPK/PGC-1α/GLUT4 signaling pathways to enhance energy metabolism in chronic ischemic HF [28]. Additionally, YXS markedly modulates mitochondrial biogenesis and OXPHOS [29]. Network pharmacology has identified 34 YXS-targeted proteins predominantly involved in cardiovascular and immune system functions, including immune responses, blood coagulation, circulation, and vasodilation [30]. YXS is primarily composed of Ginseng and Astragalus. Ginsenosides, the active constituents of Ginseng, a key TCM herb for cardiovascular diseases, exert protective effects against HF by enhancing energy metabolism through AMPK and peroxisome proliferator-activated receptor (PPAR) signaling pathways [31]. Similarly, Astragalus exerts therapeutic effects in HF *via* a multi-component, multi-target mechanism [32]. Astragaloside IV, a major active ingredient in Astragalus, protects against HF by enhancing energy metabolism through PPARα activation, thereby promoting fatty acid β-oxidation [33]. Collectively, these findings indicate that YXS regulates myocardial energy metabolism; however, the precise mechanisms and active ingredients responsible for these effects remain unclear.

In the present study, we aimed to investigate the cardioprotective effects of YXS and elucidate its underlying mechanism in improving energy metabolism in a post-MI HF rat model. Our results demonstrated that YXS improved cardiac function, reduced HF biomarkers, enhanced hemodynamics, and attenuated inflammation and collagen deposition in post-MI HF rats. In-depth mechanistic analyses revealed that YXS exerts its protective effects by inhibiting the FOXO1/PDK4 signaling pathway, up-regulating oxoglutarate dehydrogenase (OGDH) expression in the TCA cycle, increasing ATP production, and thereby restoring energy metabolism. Single-cell ribonucleic acid sequencing (RNA-seq) analysis further confirmed a strong association between HF and dysregulated energy metabolism. Moreover, we performed molecular docking and *in vitro* experiments on both circulating components and major constituents of the principal herbs to identify the active ingredients responsible for YXS-mediated effects. These findings provide a theoretical foundation for future clinical applications and highlight the therapeutic potential of YXS in post-MI HF through its unique mechanism of inhibiting FOXO1/PDK4 signaling to enhance cardiac energy metabolism.

2. Materials and methods

2.1. Chemicals and drugs

YXS was provided by Qingdao Growful Pharmaceutical Co., Ltd. Sacubitril/valsartan (Sac/Val) was purchased from Novartis Co., USA. Calycosin, calycosin-7-O-beta-*D*-glucoside, cryptotanshinone, daidzein, senkyunolide H, apigenin, tanshinone II, (S)-tetrahydrocolumbamine, ginsenoside Rg1, ginsenoside Rb1, ginsenoside Rb2, ginsenoside Rc, ginsenoside Rd, ginsenoside Re, ginsenoside Rf, astragaloside III, astragaloside IV, and astragaloside VII were purchased from Sichuan Vicky Biotechnology Co., Ltd. (Chengdu, China). Sodium dichloroacetate (DCA) was obtained from MCE (HY-Y0445A). AS1842856 (HY-100596) and trimetazidine (HY-B0968A) were also procured from MCE.

2.2. Animal model

Male Sprague-Dawley rats (about 220 g, 8-week-old) were obtained from SPF Biotechnology Company Ltd. (Beijing, China). The rats were housed in the Animal Center at Tianjin University of Traditional Chinese Medicine under standard environmental conditions and provided with a standard chow diet and water *ad libitum* (No. TCM-LAEC2023218g3390; Date, February 20th, 2023). General anesthesia was induced using isoflurane.

Left anterior descending (LAD) coronary artery ligation surgery was performed to induce HF following MI. After surgery, rats received intramuscular penicillin (105 $U \cdot d^{-1}$) for 7 days and were allowed access to food and water. After a standard feeding period of 2 weeks, echocardiography revealed that LVEF was < 50%, confirming the successful establishment of a post-MI model of HFrEF.

The rats were divided into six groups: Sham, Mod, YXS L, YXS M, YXS H, and Sac/Val. YXS was crushed and suspended in saline. Rats in the low-, middle-, and high-dose groups received daily intragastric administration of YXS at 240, 480, and 960 $mg \cdot kg^{-1}$, respectively. The positive control group received 36 $mg \cdot kg^{-1} \cdot day^{-1}$ of Sac/Val, equivalent to the clinical dose. An equal volume of saline was administered to the model group. Treatment was initiated after model confirmation and continued for four weeks, after which heart tissue and blood samples were collected for analysis.

2.3. Echocardiography

Echocardiography was performed using a Vevo 2100 ultra-

sonography system (VisualSonics) with heart rate maintained at approximately 400 bpm. Cardiac function parameters were determined by averaging measurements from three consecutive cardiac cycles.

2.4. Hemodynamics

Hemodynamic assessment provides critical insights for managing complex HF. Following isoflurane anesthesia, a microtip pressure-conductance catheter (SPR-869; Millar Instruments, Houston, TX, USA) was inserted into the right carotid artery and advanced into the ascending aorta. After stabilization of heart rate and mean arterial pressure, the catheter was advanced into the left ventricle. Pressure and volume signals were continuously recorded using a pressure-volume (P-V) conductance system connected to a PowerLab data acquisition system (ML870; AD Instruments, USA).

2.5. Exercise tolerance test

Exercise tolerance was evaluated using a treadmill (Zhishuduobao Biological, Beijing, China). Rats were acclimated for 3 days by running 10 min at 10 m·min^{-1}. The formal test began at 10 m·min^{-1}, with speed increased by 4 m·min^{-1} every 3 min until exhaustion. Time to exhaustion and total distance were recorded.

2.6. Quantitative polymerase chain reaction (qPCR) analysis

Heart tissue was homogenized, and total RNA was extracted using TRIzol reagent. RNA was reverse-transcribed to complementary deoxyribonucleic acid (cDNA) (Abclonal, Wuhan, China), and qPCR was performed on a CFX Connect™ Real-Time System (Bio-Rad, USA). Primer sequences are listed in Table S1. Relative mRNA expression was calculated using the $2^{-\triangle\triangle CT}$ method with glyceraldehyde-3-phosphate dehydrogenase (GAPDH) as the reference gene.

2.7. Histological assessment

Hearts were fixed in 10% formalin for 72 h, paraffin-embedded, and sectioned at 5 μm. Tissue morphology was evaluated using hematoxylin-eosin (H&E) staining, and collagen deposition was assessed with Masson's trichrome staining [34].

2.8. Enzyme-linked immunosorbent assay (ELISA)

Plasma N-terminal pro-brain natriuretic peptide (NT-proBNP) levels were measured using an ELISA kit (ColorfulGene Biological, Wuhan, China). ANP and BNP concentrations were determined with a specific ELISA kit (JONLNBIO, Shanghai, China). Tumor necrosis factor α (TNF-α), interleukin (IL)-1β, and IL-6 were quantified using ELISA kits (JONLNBIO, Shanghai, China) [35].

2.9. Metabolome analysis

Plasma samples from the Sham, Mod, and YXS M groups were analyzed using an ultra-high performance liquid chromatography (UPLC)/Q-Exactive-Orbitrap mass spectrometry (MS) system (Thermo Fisher Scientific, MA, USA). Metabolite separation was achieved on a Waters ACQUITY UPLC HSS T3 column (2.1 mm × 100 mm, 1.8 μm). MS employed an ESI source in both positive and negative ionization modes, operating in Full MS/dd-MS2 (TopN) scan mode. The MS^1 scan range was *m/z* 100–1500 (resolution: 120 000), and the MS^2 range was *m/z* 200–2000 (resolution: 150 000). A dynamic exclusion time of 10.0 s and an isolation window of *m/z* 2.0 were applied [36]. Differential metabolites were selected based on fold change (FC > 1.2 or FC < 0.83) and *P*-value < 0.05.

2.10. RNA-seq analysis

RNA-seq was performed on five randomly selected heart samples per group (Sham, Mod, YXS M) by LC-BIO Biotech Ltd. (Hangzhou, China). Libraries were sequenced on an Illumina NovaSeq™ 6000 platform, generating 2 × 150 bp paired-end reads. Differentially expressed genes (DEGs) were defined as $|\log_2 foldchange| > 1$ and *P*-value < 0.05. Gene Set Enrichment Analysis (GSEA) was conducted using http://www.broadinstitute.org/gsea/index.jsp.

2.11. Detection of ATP and lactic acid (LA) levels

ATP levels (Beyotime, Shanghai, China) were measured in heart tissue (10–20 mg) or H9c2 cells. LA concentrations were determined in 10–20 mg of heart tissue (Solarbio, Beijing, China).

2.12. Western blot analysis

Heart tissue was lysed in RIPA buffer, and protein concentrations were quantified. Primary antibodies included: FOXO1 (A2934; Abclonal, China), OGDH (A22163; Abclonal, China), PDK4 (ab214938; Abcam, UK), and GAPDH (HC301; TransGen Biotech, China). Blots were imaged using an Amersham Imager 600 (GE Healthcare Bio-Sciences AB, Sweden).

2.13. Single-cell RNA-seq analysis

Dilated cardiomyopathy (DCM) datasets were retrieved from the NCBI GEO repository (http://www.ncbi.nlm.nih. gov/geo) using the terms "heart failure", "snRNA-seq", and "scRNA-seq". Nuclei data from dataset GSE183852 were selected for analysis [37]. Data processing was performed using Seurat v5.3.0. The gene expression matrix was normalized *via* LogNormalize and subjected to principal component analysis (PCA). Gene ontology enrichment was conducted with clusterProfiler (v4.0) using human genome annotation (organism = "hsa") and a significance threshold of *P*.adjust < 0.05. GSEA was applied to assess pathway alterations in cardiomyocytes, with differential expression between DCM and donor samples calculated using the Wilcoxon rank sum test in Seurat (logfc.threshold = 0.01). Gene symbols were converted to ENTREZIDs *via* org.Hs.eg.db, and the MSigDB hallmark gene set (v7.5.1) was obtained using msigdbr. GSEA significance was set at pvalueCutoff = 0.1.

2.14. Molecular docking

X-ray crystal structures of human FOXO1, PDK4, and the OGDH pleckstrin homology domain (PDB IDs: 4LG0, 7EBG, and 8I0K) were downloaded from the Protein Data Bank (http://www.rcsb.org/). Compound structures were sourced from PubChem (https://pubchem.ncbi.nlm.nih.gov/). Proteins were prepared for docking using Discovery Studio Client (2019) and AutoDock Vina [38]. Binding affinities were evaluated based on the lowest binding energies, and predicted inhibition constants (pKi) were derived from docking log files (dlg). Mean binding energies ± standard error of the mean (SEM) were calculated from three independent docking runs. Interactions were visualized using PyMOL.

2.15. Cellular thermal shift assay (CETSA)

H9c2 cells or heart tissue lysates were subjected to three freeze-thaw cycles in liquid nitrogen. Lysates were split into two

aliquots and treated with either DMSO or 10 μmol·L^{-1} apigenin for 30 min. After heating at 42–62 °C for 5 min and immediate cooling on ice, samples were analyzed by Western blot.

2.16. Oxygen-glucose deprivation (OGD)-stimulated H9c2 cells

H9c2 cells were seeded at about 5000 cells/100 μL or 10^4 cells/mL in 96- or 6-well plates and incubated for 12 h. The medium was replaced with fresh medium containing various concentrations of YXS or its individual components. After 24 h of pretreatment, the medium was switched to glucose-free Dulbecco's modified Eagle medium (DMEM) without fetal bovine serum (QriCell Biotech, Guangzhou, China). Cells were then placed in an anaerobic chamber (95% N_2, 5% CO_2) at 37 °C for 14 h (Thermo Fisher Scientific, America) to establish the OGD-induced injury model.

2.17. Cell viability analysis

Briefly, 10 μL of CCK-8 reagent (APExBIO, USA) was added to each well, followed by incubation at 37 °C for 40 min. Absorbance was measured at 450 nm, and cell viability in the treatment or OGD groups was expressed relative to the control group.

2.18. PDH and α-ketoglutarate dehydrogenase (α-KGDH) activity assays

The cellular PDH activity was measured using a PDH Activity Assay Kit (BC0385; Solarbio, China), while cellular α-KGDH activity was quantified using the α-KGDH Activity Assay Kit (BC0715; Solarbio, China).

2.19. Chromatin-immunoprecipitation-qPCR (ChIP-qPCR)

ChIP-qPCR was conducted using a reagent kit (RK20258; Abclonal, China). To facilitate cross-linking of proteins to DNA, H9c2 cells were treated with 1% formaldehyde. The cells were lysed in the presence of protease inhibitors and sonicated to induce DNA fragmentation. The resulting mixture was then incubated with an antibody specific for FOXO1 (2880; Cell Signaling Technology, MA, USA) or IgG (negative control). Target DNA fragments were quantified using qPCR. The primers targeting the PDK4 promoter were as follows: forward 5'-CAGCTGCTGGACTTCGGTAA-3' and reverse 5'-AGGCTTCTGGGTTCTTCAGC-3'.

2.20. Analysis of mitochondrial respiration and energy metabolism

Mitochondrial respiration was assessed using the Seahorse XFp Cell Mito Stress Test. XF Base Medium was used instead of DMEM. The appropriate compounds were loaded onto suitable ports of a hydrated sensor cartridge at the following final concentrations: oligomycin (10 μmol·L^{-1}), FCCP (10 μmol·L^{-1}), and a mixture of rotenone (5 μmol·L^{-1}) and antimycin A (10 μmol·L^{-1}) (103015-100; Agilent, USA).

2.21. Data analysis

Statistical analysis was conducted using SPSS version 21.0 (IBM Corp., Armonk, NY, USA). Data were first subjected to normality testing (Shapiro-Wilk test) and homogeneity of variance testing. For continuous data that followed a normal distribution, results are expressed as mean ± SEM, and intergroup comparisons were performed using one-way ANOVA. When the assumption of homogeneity of variance was met, the LSD method was used for post-hoc pairwise comparisons; when the assumption was violated, Dunnett's T3 method was employed. For continuous data that did not follow a normal distribution, results are presented as median (interquartile range), and intergroup comparisons were conducted using non-parametric tests.

3. Results

3.1. YXS improves cardiac function and exercise endurance in HF post-MI

To evaluate the effect of YXS on post-MI HF, rat HF models were constructed using LAD ligation. Rats with LVEF <50% after 2 weeks were considered successful models, and YXS was administered for 4 weeks (Fig. 1A). In the Mod group, LVEF and left ventricular fractional shortening (LVFS) values were significantly reduced, whereas left ventricular end-systolic volume (LV Vols), left ventricular end-diastolic volume (LV Vold), and left ventricular internal dimensions in end-systole and end-diastole (LVIDs and LVIDd, respectively) were significantly elevated, while interventricular septum thickness at end-systole (IVSs) and left ventricular posterior wall thickness in systole (LVPWs) were considerably reduced. After YXS administration for 2 weeks, LVEF and LVFS were significantly increased in the YXS M and YXS H groups, while LV volumes and LVID were decreased. Sac/Val, as a positive control, significantly increased LVEF and LVFS values (Figs. 1B–1F and Figs. S1A–1F). However, YXS treatment did not significantly improve movement distance and time in the exercise tolerance test (Figs. 1G–1H).

Next, we assessed the effects of YXS administration for 4 weeks. In the Mod group, LVEF and LVFS were further reduced, indicating progression of HF severity over time. After 4 weeks of YXS treatment, LVEF and LVFS were significantly increased in the YXS M and YXS H groups, accompanied by improvements in LV volumes, LVID, IVSs, and LVPWs, indicating that YXS effectively alleviates cardiac dysfunction (Figs. 1I–1M and Figs. S1G–1L). Movement distance and time significantly improved, indicating that YXS enhances exercise endurance in rats with HF (Figs. 1N–1O). Sac/Val, the positive control, improved cardiac function. These results indicated that YXS improved cardiac function and exercise endurance in rats with post-MI HF.

3.2. YXS improves hemodynamics, HF biomarkers, and cardiac pathology in post-MI HF

The P-V loop reveals ventricular hemodynamic changes during ejection by illustrating the relationship between ventricular pressure and volume throughout the cardiac cycle [39]. Treatment with YXS improved the Tau constant and ± dp/dt max in rats (Figs. 2A–2D). YXS also reduced the levels of HF biomarkers, including ANP, BNP, and NT-proBNP (Figs. 2E–2G). Additionally, our research findings indicate that YXS significantly reduces serum levels of ANP, BNP, and NT-proBNP, thereby ameliorating HF. Furthermore, YXS lowers the levels of inflammatory markers TNF-α, IL-6, and IL-1β, alleviating inflammation (Fig. S2). Examination of H&E-stained sections revealed that YXS improved the arrangement of cardiac muscle fibers and reduced inflammatory cell infiltration (Fig. 2I). Masson staining demonstrated markedly reduced cardiac fibrosis in the YXS M and H groups (Figs. 2H, 2J). These results further confirmed that YXS protects against post-MI HF.

3.3. YXS regulates energy metabolism

To explore the mechanism of action of YXS, we conducted a metabolomics study and identified 40 differentially expressed metabolites (Fig. S3, Fig. 3A, Table S2). Enrichment analysis of the differential metabolites revealed that the TCA cycle was the primary affected pathway (Fig. 3B). In mitochondria, the TCA cycle and OXPHOS are central to cellular energy metabolism. Moreover, the oxidation of sugars, lipids, and amino acids ulti-

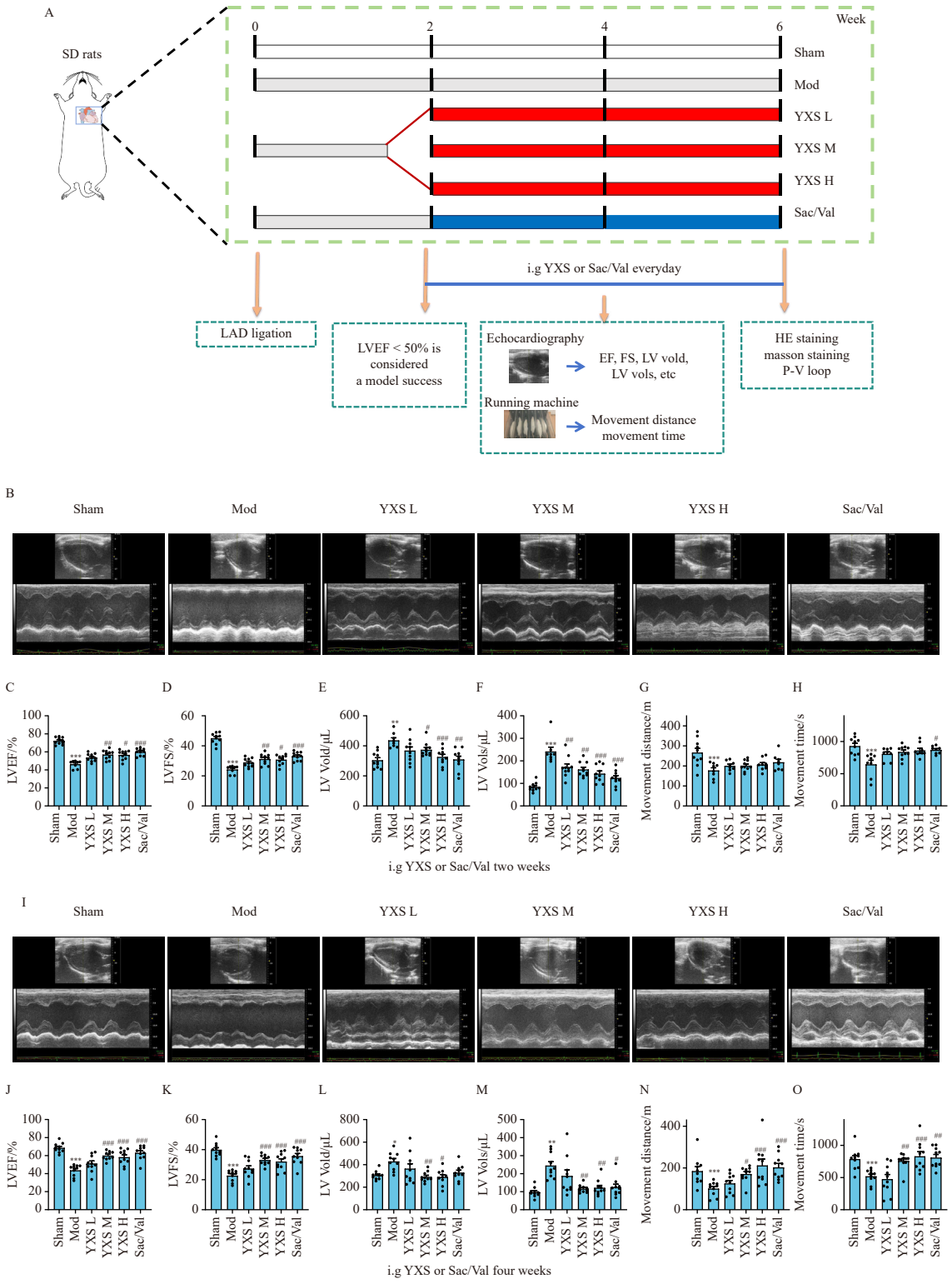

Fig. 1 YXS improves cardiac function and exercise endurance in post-myocardial infarction heart failure. Male Sprague–Dawley rats are subjected to LAD ligation, then treated with different doses of YXS for 2 and 4 weeks, respectively. (A) A flow chart illustrating the pharmacodynamic study design. (B) Representative ultrasonic image of cardiac function at 2 weeks post-YXS treatment. (C–F) Quantitative analysis of LVEF, LVFS, LV Vold, and LV Vols at 2 weeks post-YXS treatment. (G–H) Treadmill-assessed movement distance and movement time at 2 weeks post-YXS treatment. (I) Representative ultrasonic image of cardiac function at 4 weeks post-YXS treatment. (J–M) Quantitative analysis of LVEF, LVFS, LV Vold, and LV Vols at 4 weeks post-YXS treatment. (N–O) Treadmill-assessed movement distance and movement time at 4 weeks post-YXS treatment. Data are analyzed using one-way ANOVA with LSD post-hoc test after confirmation of homogeneity of variance. Data are expressed as mean ± SEM (n = 8–10). $^{*}P < 0.05$, $^{**}P < 0.01$, $^{***}P < 0.001$ *vs* Sham group; $^{\#}P < 0.05$, $^{\#\#}P < 0.01$, $^{\#\#\#}P < 0.001$ *vs* Mod group. LV, left ventricle; LVEF, left ventricular ejection fraction; LVFS, left ventricular fractional shortening; YXS, Yangxinshi Tablet

mately converges into the TCA cycle, enabling these substrates to support bioenergy production, biosynthesis, and redox homeostasis [40]. Analysis of RNA levels of key TCA cycle-related genes revealed changes in PDK4, HK2, and SLC2A1 in the glucose metabolism pathway; OGDH and SUCLG1 in the TCA cycle pathway; and UCP2 and UCP3 genes in the OXPHOS pathway. These results suggest that YXS modulates the TCA cycle by regulating PDK4 activity in glucose metabolism (Figs. 3C–3F). Treatment with YXS significantly increased OGDH protein expression (Figs. 3G–3H). Moreover, YXS increased ATP levels, which reflect OXPHOS activ-

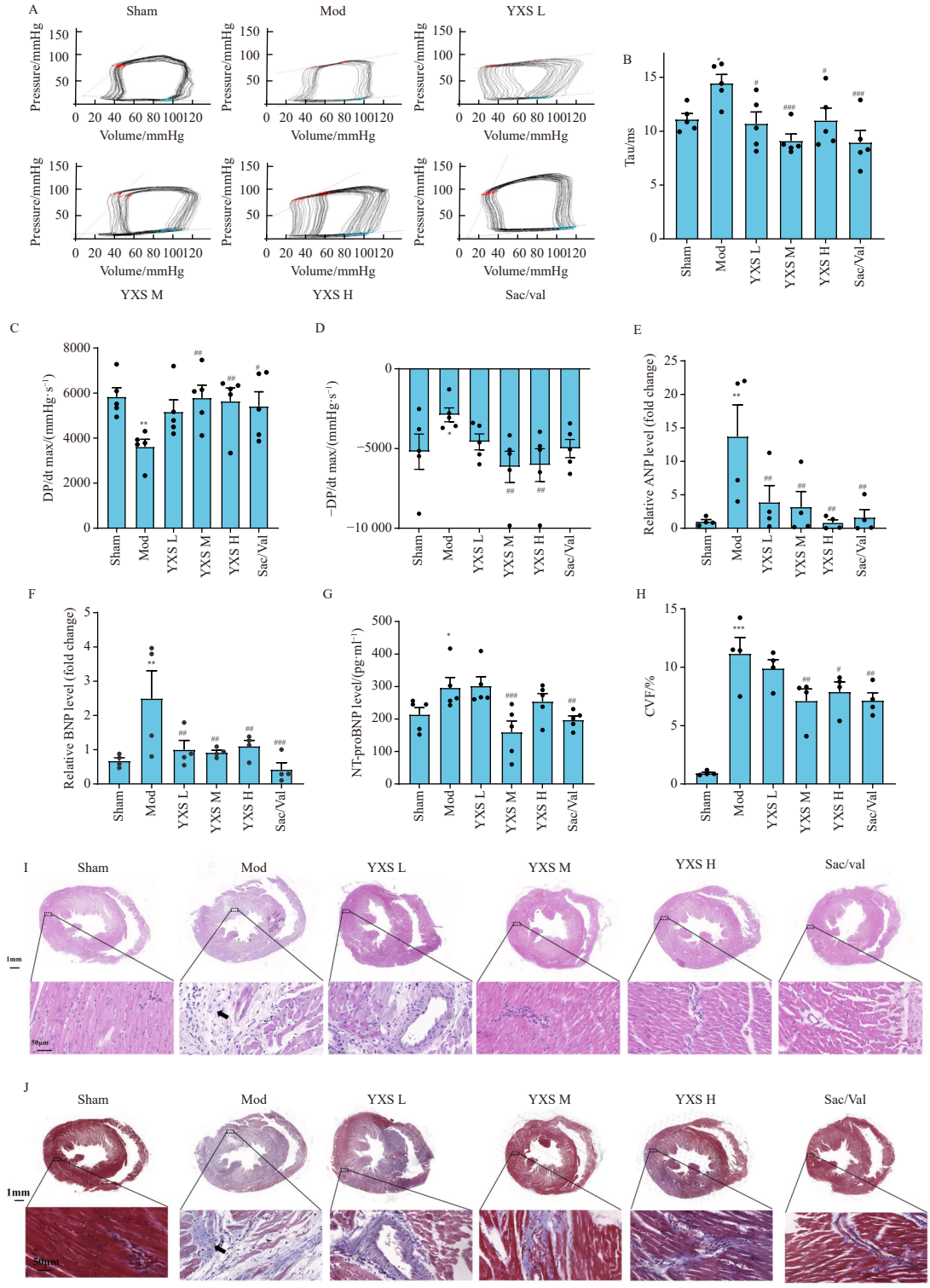

Fig. 2 YXS improves hemodynamics, heart failure biomarkers, and cardiac pathology in post-myocardial infarction heart failure. (A) Representative ultrasonic image of the P-V loop at 4 weeks post-YXS treatment. (B–D) Quantitative analysis of the dp/dt max, -dp/dt max, and TAU at 4 weeks post-YXS treatment. (E–G) Levels of ANP, BNP, and NT-proBNP at 4 weeks post-YXS treatment. (I) Representative images of hematoxylin-eosin-stained sections at 4 weeks post-YXS treatment. (H, J) Representative diagram and statistical analysis of Masson-stained sections at 4 weeks post-YXS treatment. Data are analyzed using one-way ANOVA with LSD post-hoc test after confirmation of homogeneity of variance. Data are expressed as mean ± SEM (n = 4–5). $^{*}P < 0.05$, $^{**}P < 0.01$, $^{***}P < 0.001$ *vs* Sham group; $^{\#}P < 0.05$, $^{\#\#}P < 0.01$, $^{\#\#\#}P < 0.001$ *vs* Mod group. ANP, atrial natriuretic peptide; BNP, brain natriuretic peptide; YXS, Yangxinshi Tablet.

ity, while decreasing lactate levels, a marker of glycolytic metabolism (Figs. 3I–3J). Collectively, YXS regulates cellular energy metabolism by enhancing the TCA cycle (Fig. 3K).

3.4. YXS inhibits FOXO1/PDK4 signaling

To gain a comprehensive transcriptional perspective of the effects of YXS on HF, RNA-seq analysis was performed, identifying 186 DEGs across the three groups, including 96 up-regulated and 90 down-regulated in the YXS group (Figs. 4A–4B). Furthermore, compared with the YXS group, the Mod group exhibited 837 DEGs, including 344 upregulated and 493 downregulated genes (Fig. 4C). The transcriptome results were verified by qPCR, showing trends consistent with the sequencing results (Fig. S4).

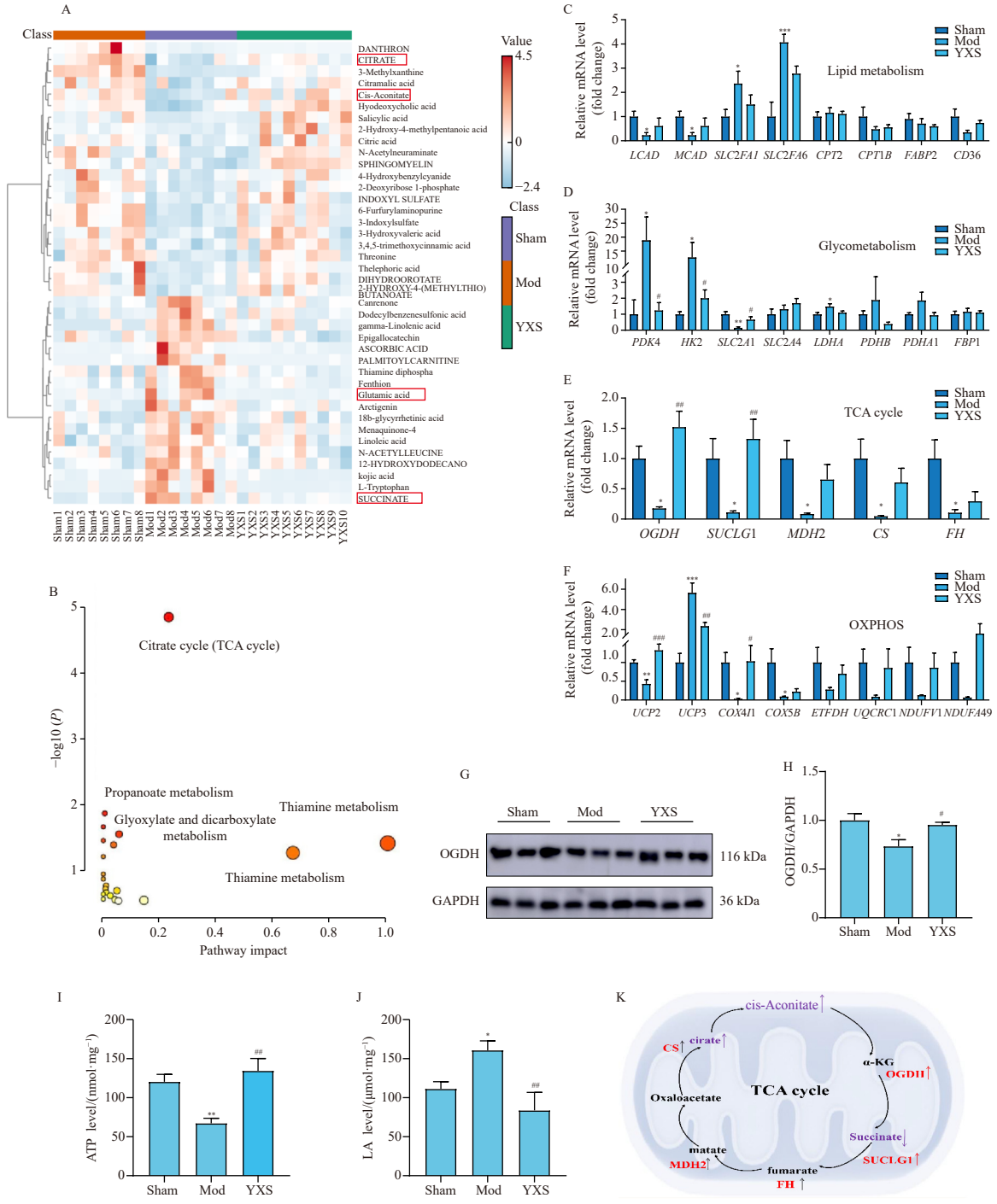

Fig. 3 YXS regulates energy metabolism. (A) Representative heatmap of differential metabolites in plasma samples from the Sham, Mod, and YXS M groups. (B) Bubble map of differential metabolites (n = 8–10). (C–F) mRNA expression levels of the key genes involved in glucose metabolism, the TCA cycle, fatty acid metabolism, and oxidative phosphorylation. (G–H) Western blot analysis of the cardiac oxoglutarate dehydrogenase protein. (I–J) Levels of ATP and LA in the heart. Scale bar: 50 μm. (K) Schematic diagram illustrating metabolites and genes altered in the TCA cycle (n = 3). Data are analyzed using one-way ANOVA with LSD post-hoc test after confirmation of homogeneity of variance. Data are expressed as mean ± SEM. $^{*}P < 0.05$, $^{**}P < 0.01$, $^{***}P < 0.001$ *vs* Sham group; $^{\#}P < 0.05$, $^{\#\#}P < 0.01$, $^{\#\#\#}P < 0.001$ *vs* Mod group.

GSEA analysis indicated that YXS exerts its actions through the FOXO pathway, with the gene set significantly down-regulated (Figs. 4D–4E). FOXO transcription factors are known to regulate energy metabolism [41]. Western blot analysis was performed to further verify the protective mechanisms of YXS. The Mod group exhibited markedly higher FOXO1 and PDK4 expression than the Sham group, and these levels were significantly reduced by YXS treatment (Figs. 4F–4H). Immunofluorescence analysis revealed that FOXO1 expression was significantly enhanced after OGD induction. In contrast, YXS significantly decreased FOXO1 expression (Figs. 4I–4J). ChIP-qPCR further confirmed that FOXO1 functions as a transcription factor for PDK4 (Figs. 4K–4L). These results suggest that YXS exerts its protective effects by inhibiting FOXO1/PDK4 signaling.

3.5. Energy metabolism is closely associated with HF

To further validate our experimental results, we selected datasets from healthy individuals and patients with DCM and conducted single-cell RNA-seq analysis based on the literature. Unsupervised clustering of the single-cell RNA-seq data identified multiple cardiac cell clusters, with characteristic cell marker gene expression consistent with prior reports (Figs. 5A–5B) [37]. Kyoto Encyclopedia of Genes and Genomes (KEGG) pathway ana-

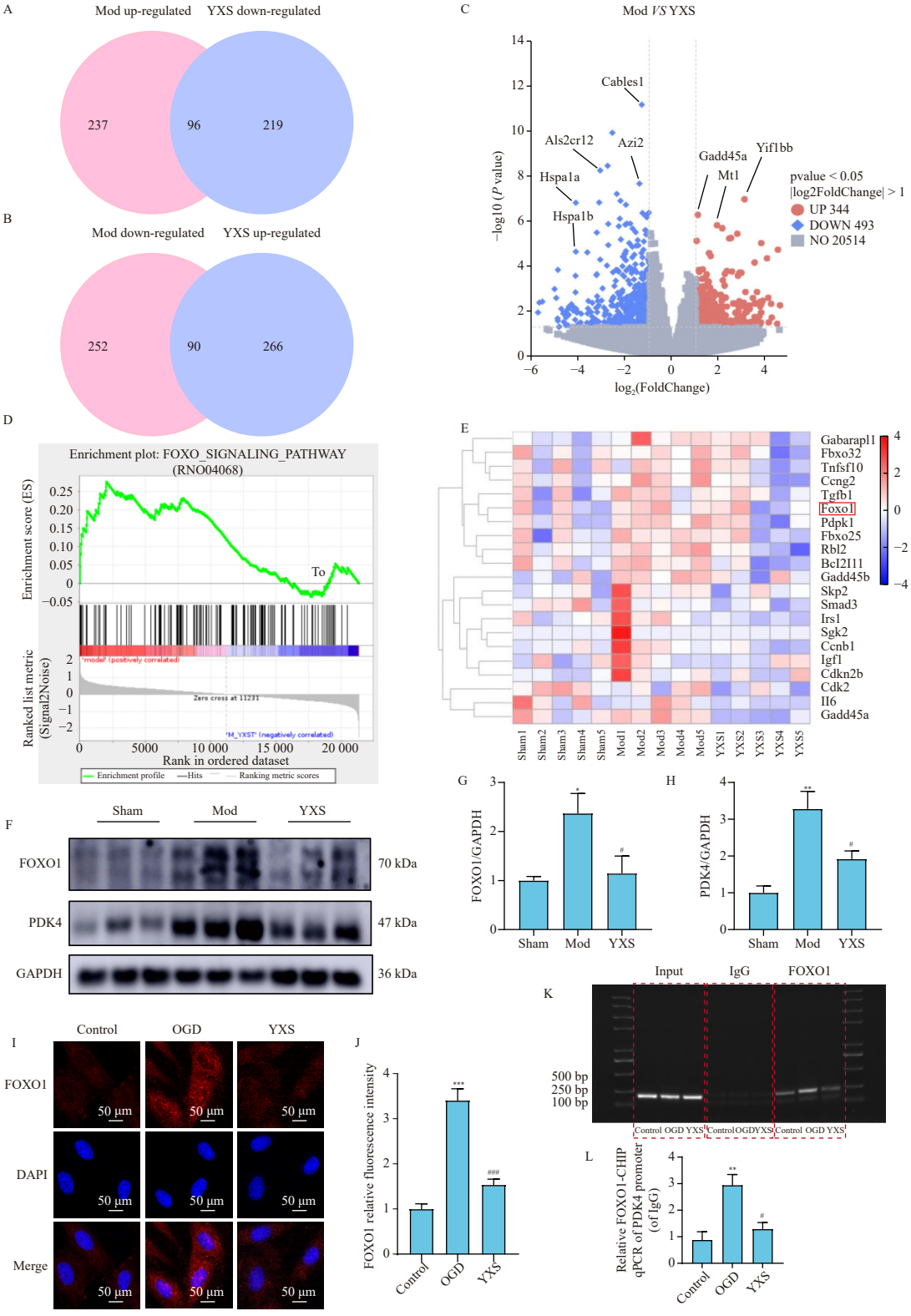

Fig. 4 YXS inhibits FOXO1/PDK4 signaling. (A–B) Venn diagrams of heart samples from the Sham, Mod, and YXS M groups. (C) Volcano plot comparing the Mod and YXS-M groups. (D–E) GSEA and cluster analyses of genes involved in the FOXO signaling pathway (n = 5). (F–H) Western blot analysis of cardiac FOXO1 and PDK4 protein expression. (I–J) Immunofluorescence analysis of FOXO1 expression in YXS-treated H9c2 cells. Scale bar = 50 μm. (K) Agarose gel electrophoresis showing the predicted binding sequences in FOXO1 antibody IP, IgG, and input samples. (L) qPCR quantification of the enrichment levels of binding sequences in the FOXO1-ChIP and IgG groups (n = 3). Data are analyzed using one-way ANOVA with LSD post-hoc test after confirmation of homogeneity of variance. Data are presented as mean ± SEM. $^{*}P < 0.05$, $^{**}P < 0.01$, $^{***}P < 0.001$ *vs* Sham group; $^{\#}P < 0.05$, $^{\#\#\#}P < 0.001$ *vs* Mod group. GSEA, gene set enrichment analysis; YXS, Yangxinshi Tablet.

lysis was subsequently conducted on these clusters (Fig. 5C). GSEA analysis of the identified genes revealed that OXPHOS was closely related to HF (Fig. 5D). The OXPHOS process is linked to energy metabolism and metabolic processes. Moreover, expression of OXPHOS-related genes was reduced. We also observed changes in FOXO1 and PDK4 in cells, with their expression upregulated in the cardiomyocytes of patients with HF, consistent with our experimental findings (Figs. 5E–5F). The change in PDK4 was particularly pronounced, consistent with our experimental results.

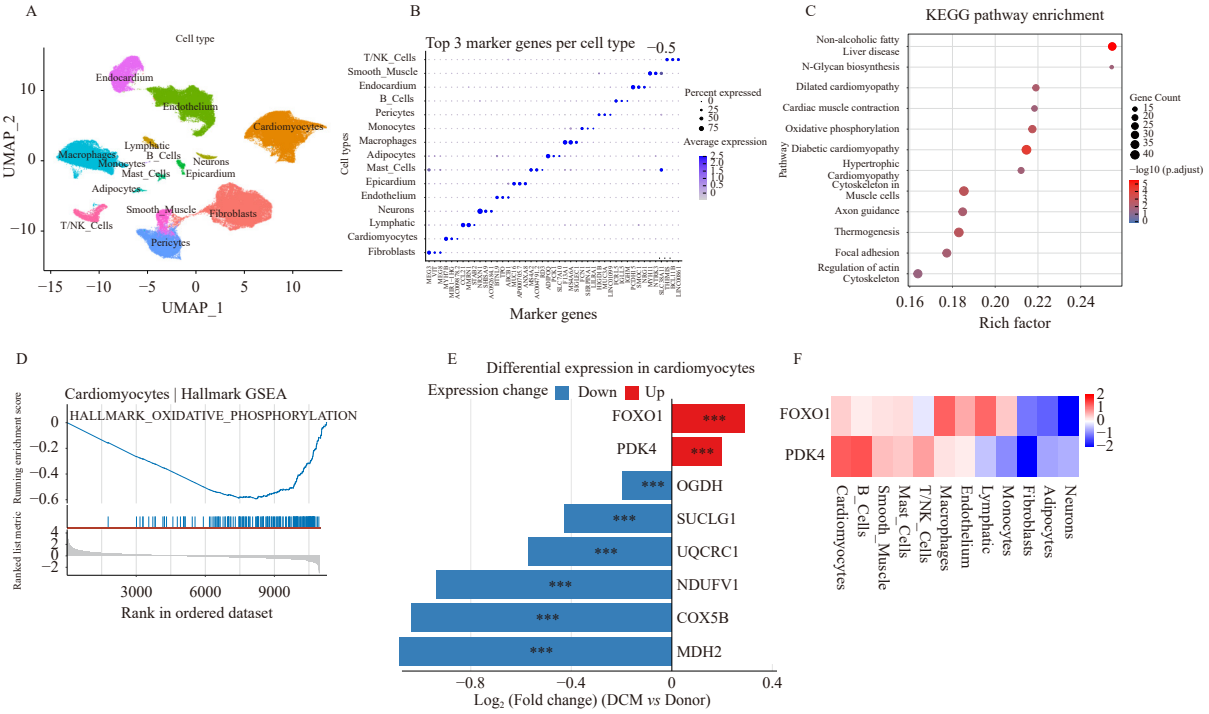

Fig. 5 Energy metabolism is closely related to heart failure. (A) Unsupervised clustering of single-cell RNA sequencing data. (B) Expression of characteristic cell marker genes in the single-cell RNA sequencing datasets. (C) KEGG analysis. (D) GSEA analysis in cardiomyocytes. (E) Changes in genes in cardiomyocytes. (E) Changes in *FOXO1* and *PDK4* expression levels in the cells. GSEA, gene set enrichment analysis; KEGG, Kyoto Encyclopedia of Genes and Genomes

3.6. YXS regulates mitochondrial energy metabolism via the FOXO1/PDK4 pathway

To further investigate the mechanism of action of YXS, OGD-stimulated H9c2 cells were used to mimic hypoxic HF, and mitochondrial respiration was examined using the Agilent Seahorse XFp Cell Mito Stress Test. H9c2 cells were pretreated with YXS for 24 h before OGD induction. The OGD group exhibited reductions in basal respiration, ATP production, and maximal respiration, suggesting mitochondrial energy metabolism dysfunction. Conversely, treatment with YXS (200 μg·mL^{-1}) elevated basal respiration, ATP production, and maximal respiration (Figs. 6A–6D). PDK4 is a key regulator of PDH activity [42]. Subsequently, we detected cell viability, ATP levels, and PDH enzyme activities following YXS treatment, which revealed that YXS (200 μg·mL^{-1}) improved energy metabolism and cell survival (Figs. 6E–6G). Subsequently, cell viability, ATP levels, and PDH enzyme activity were determined after treatment with the PDK inhibitor DCA (Figs. 6H–6J) or FOXO1 inhibitor AS1842856 (Figs. 6K–6M). Interestingly, DCA and AS1842856 enhanced H9c2 cell viability, ATP levels, and PDH enzyme activity, with no significant additional enhancement observed upon co-treatment with YXS.

To further investigate the mechanism of YXS in combating HF, we constructed FOXO1 small interfering RNA (siRNA) and overexpression vectors. The results showed that after overexpression of *FOXO1*, ATP and PDH levels in OGD-induced cardiomyocytes significantly decreased following YXS administration (Figs. 7A–7C). Conversely, after administration of *FOXO1* siRNA, ATP and PDH levels in OGD-induced injured cardiomyocytes significantly increased, demonstrating the direct regulatory effect of YXS on FOXO1 (Figs. 7D–7F). The H9c2 cell line represents features of cardiac myoblasts [43]; therefore, we extracted primary cardiomyocytes from neonatal rats aged 1 to 3 days to further validate our experimental results. We administered YXS to primary cardiomyocytes after OGD induction, demonstrating that YXS has a protective effect on primary cardiomyocytes, capable of improving the decline in ATP content and PDH activity. Furthermore, the addition of DCA and AS1842856 enhanced ATP levels and PDH enzyme activity in primary cardiomyocytes, while co-treatment with YXS did not show a significant additional enhancement effect. This result is consistent with our previous findings (Figs.7G–7L). These findings suggest that YXS enhances mitochondrial energy metabolism by inhibiting the FOXO1/PDK4 signaling pathway.

3.7. Main components regulating FOXO1 transcription

To identify the active constituents of YXS that regulate energy metabolism, we analyzed the blood components of YXS, along with the main components of Ginseng and Astragalus. First, the total ion chromatogram was obtained, and 16 blood compounds were identified in both positive and negative ion modes (Fig. 8A, Table S3). Second, we selected eight saponins from Ginseng and Astragalus for further investigation (Fig. 8B). Finally, all 32 compounds were subjected to molecular docking analysis with FOXO1, PDK4, and OGDH (Figs. 8C–8E, Tables S4–S5). Based on the binding affinities of the compounds to the selected targets, the most promising compounds were selected for subsequent cell experiments.

After molecular docking, all compounds were ranked according to their binding affinities to the selected proteins. We selected the common compounds with the top sixteen binding energies for each protein [44]. Eight compounds with high binding energies to all three proteins were identified (Fig. 9A). For the main components of Ginseng and Astragalus, we selected seven ginsenosides and three astragaloside saponins based on their binding affinities and compound availability. Among the 18 components, senkyunolide H, apigenin, ginsenoside Rb2, ginsenoside Rg1, ginsenoside Re, ginsenoside Rf, astragaloside IV, and astragaloside VII protected against OGD-induced H9c2 cell injury (Fig. 9B). Further assessment of ATP levels revealed that senkyunolide H, apigenin, astragaloside IV, and astragaloside VII enhanced energy metabolism (Fig. 9C). The α-KGDH complex comprises OGDH, one of the key enzymes regulating the TCA cycle [45]. Activities of PDH and α-KGDH enzymes were measured, further validating the molecular docking results (Figs. 9D–9E). In addition, senkyunolide

H, apigenin, astragaloside IV, and astragaloside VII increased ATP levels and PDH activity in primary cardiomyocytes (Fig. S6). CETSA further confirmed the interactions between FOXO1, PDK4, and OGDH with apigenin (Figs. 9F–9K). PyMol maps of the four components are presented (Fig. S5). Immunofluorescence analysis further confirmed that senkyunolide H, apigenin, astragaloside IV, and astragaloside VII significantly decreased FOXO1 expression (Figs. 9L–9M).

3.8. Molecular dynamics simulations reveal differential binding stability and interaction modes of apigenin, astragaloside IV, astragaloside VII, and senkyunolide H within the PDK4 ATP-binding site

To investigate the binding stability and dynamics of potential inhibitors targeting the ATP-binding site of PDK4, we performed 500 ns molecular dynamics simulations for PDK4 in complex with four different ligands: apigenin, astragaloside IV, astragaloside VII, and senkyunolide H. Initial binding poses were obtained from prior molecular docking studies. We initially assessed the overall structural stability of the protein backbone in each complex throughout the 500 ns simulations by calculating the root-mean-square deviation (RMSD) relative to the initial structure after alignment. All four systems exhibited relatively stable backbone RMSD values for most of the simulation time, generally fluctuating around 2.0–2.5 Å (Fig. 10A). The PDK4-apigenin, PDK4-astragaloside IV, and PDK4-senkyunolide H complexes maintained this level of stability throughout the 500 ns trajectory. However, the PDK4-astragaloside VII complex showed a noticeable increase in backbone RMSD after approximately 420 ns, increasing from ~ 2.0 Å to fluctuate around 3.0 Å toward the end of the simulation, suggesting a potential conformational change in the protein structure in this specific complex during the later stages (Fig. 10A).

To evaluate the stability of the ligand binding poses within the ATP-binding site, we analyzed the persistence of contacts between the ligand and the initial set of interacting protein residues (defined as ATP-binding site residues within 4 Å of the ligand in the starting structure). Binding states were categorized based on the percentage of these initial contacts lost over time: "Bound" (0%–20% contacts lost); "Partial" (20%–80% lost); and "Unbound" (> 80% lost) (Fig. 10B). Apigenin displayed moderate stability, remaining in the "Bound" state for 28.89%, in the "Partial" state for 17.88%, and in the "Unbound" state for 53.23% of the simulation. Astragaloside IV predominantly occupied the "Partial" state (98.00%), maintaining a substantial but incomplete set of initial interactions throughout the simulation, with minimal time spent "Bound" (1.64%) or "Unbound" (0.36%). Astragaloside VII behaved similarly, residing mainly in the "Partial" state (86.34%), but also occupying the "Unbound" state for 13.62% of the time, consistent with the backbone RMSD increase observed later in its trajectory (Fig. 10A). Senkyunolide H was the least stable ligand, occupying the "Unbound" state for the vast

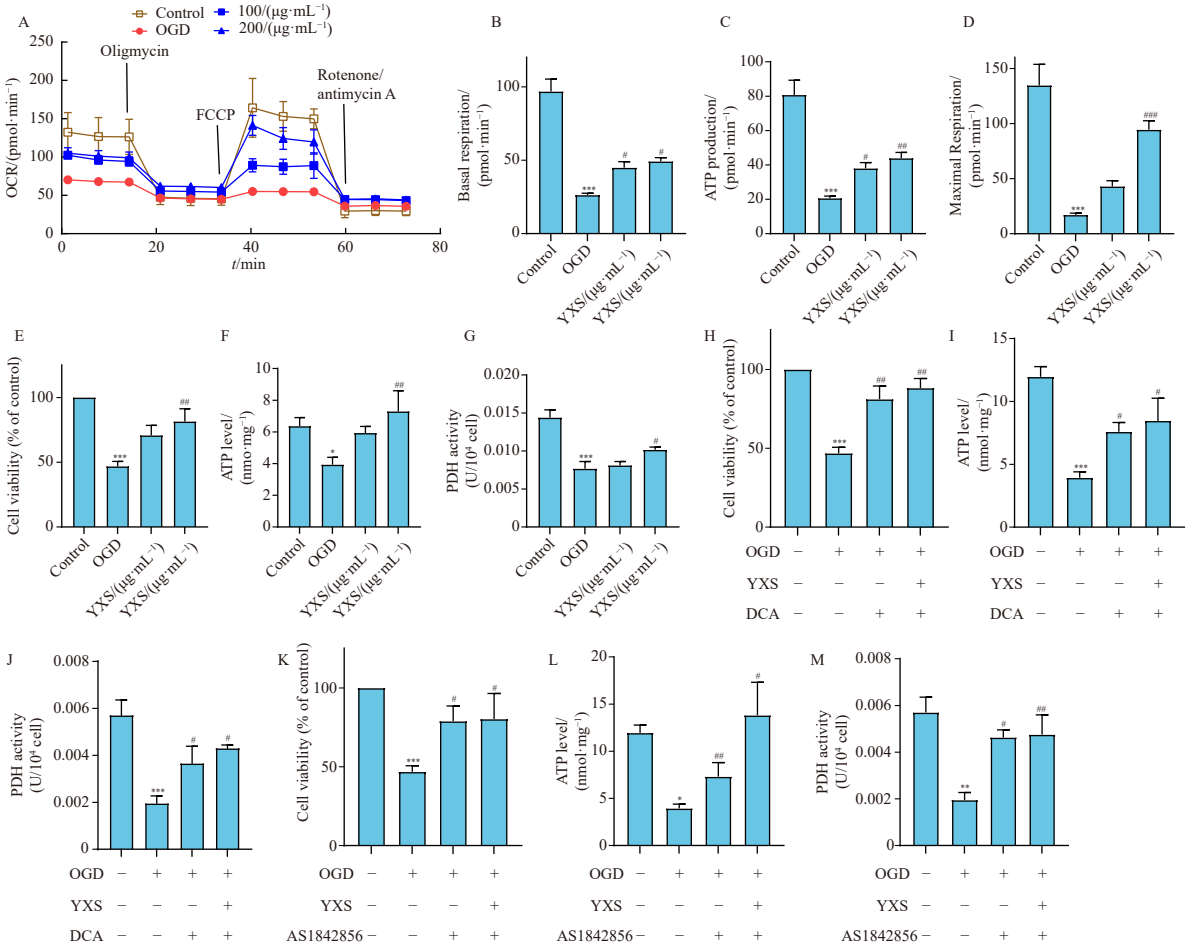

Fig. 6 YXS regulates mitochondrial energy metabolism *via* the FOXO1/PDK4 pathway. (A) Respiration profile of H9c2 cells. OCR is measured in H9c2 cells pretreated with YXS (100 and 200 μg·mL^{-1}) for 24 h and then exposed to OGD conditions. (B–E) Quantitative analysis of basal respiration, ATP production, and maximal respiration. (F–G) Cell viability, ATP level, and PDH activity of H9c2 cells pretreated with YXS (100 and 200 μg·mL^{-1}) for 24 h and then exposed to OGD conditions. (H–J) Cell viability, ATP level, and PDH activity of H9c2 cells pretreated with YXS 200 μg·mL^{-1} and DCA 10 μmol·L^{-1} for 24 h and then exposed to OGD conditions. (K–M) Cell viability, ATP level, and PDH activity of H9c2 cells pretreated with YXS 200 μg·mL^{-1} and AS1842856 10 μmol·L^{-1} for 24 h and then exposed to OGD conditions. Data are analyzed using one-way ANOVA with LSD post-hoc test after confirmation of homogeneity of variance. Data are expressed as mean ± SEM (n = 3). $^{*}P < 0.05$, $^{**}P < 0.01$, $^{***}P < 0.001$ *vs* Control group; $^{\#}P < 0.05$, $^{\#\#}P < 0.01$, $^{\#\#\#}P < 0.001$ *vs* OGD group. OCR, Oxygen consumption rate; OGD, oxygen-glucose deprivation; PDH, pyruvate dehydrogenase; YXS, Yangxinshi Tablet.

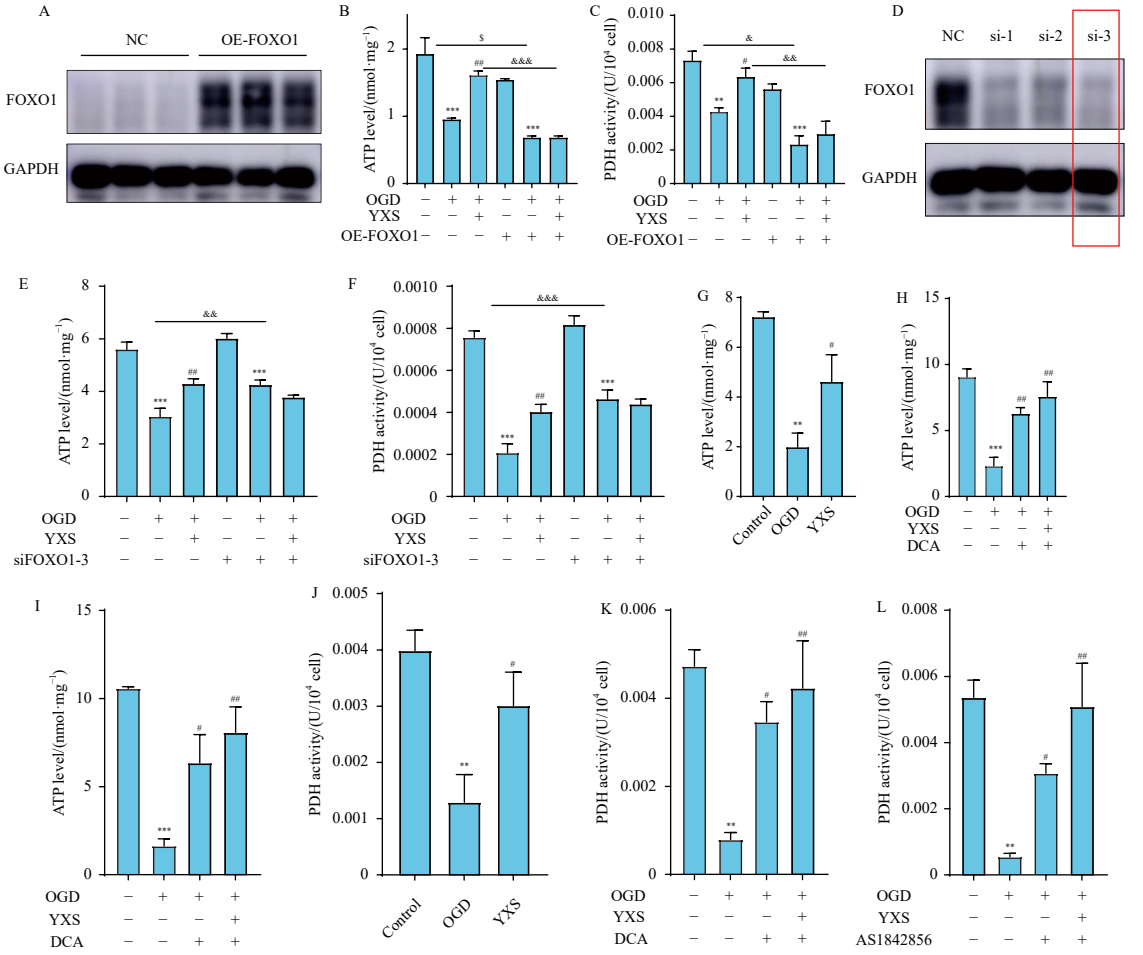

Fig. 7 FOXO1 is the direct target through which YXS exerts its protective effect. (A–C) The FOXO1 overexpression in H9c2 cell. (D–F) FOXO1 siRNA knockdown in H9c2 cells. (G–L) Changes in ATP and PDH levels in primary neonatal rat cardiomyocytes. Data are analyzed using one-way ANOVA with LSD post-hoc test after confirmation of homogeneity of variance. Data are expressed as mean ± SEM (n = 3). $^{**}P < 0.01$, $^{***}P < 0.001$ *vs* Control group; $^{\#}P < 0.05$, $^{\#\#}P < 0.01$, $^{\#\#\#}P < 0.001$ *vs* OGD group. $^{\&}P < 0.05$, $^{\&\&}P < 0.01$, $^{\&\&\&}P < 0.001$ *vs* OE-FOXO1 or SiFOXO1-3. OGD, oxygen-glucose deprivation; YXS, Yangxinshi Tablet.

majority (94.02%) of the simulation, with negligible time spent "Bound" (0.42%) or "Partial" (5.56%) (Fig. 10B) states.

Complementary to the contact analysis, ligand mobility was assessed by calculating the RMSD of the ligand heavy atoms relative to their initial docked pose after alignment of the protein backbone (Fig. 10C). The distributions of ligand RMSD values correlated well with the contact stability results. Astragaloside IV and astragaloside VII, the most stably bound ligands according to contact analysis, showed unimodal RMSD distributions centered at higher values (~ 2.1 Å and ~ 2.7 Å for astragaloside IV and VII, respectively), indicating they settled into stable conformations that slightly deviated from the initial docked pose but maintained significant protein contacts. Apigenin exhibited a bimodal RMSD distribution, with peaks at approximately 0.7 Å and 1.8 Å, reflecting its transitions between a near-initial pose ("Bound" state) and other conformations ("Partial"/"Unbound" states). Senkyunolide H, which was mostly unbound, displayed a broader RMSD distribution centered around 1.0 Å, consistent with its higher mobility and loss of specific interactions within the binding site.

To further characterize the dominant binding modes, clustering analysis was performed on the last 400 ns of each trajectory using the GROMOS algorithm, and representative structures from the most populated clusters corresponding to the "Bound" or "Partial" states were examined (Figs. 10D–10G). Analysis of these structures revealed key interactions within the PDK4 ATP-binding site, typically involving residues in the ranges 254–261, 312–313, and 329–334 [46]. For apigenin, the representative structure formed two hydrogen bonds with the backbone of Gly297, alongside hydrophobic interactions within the pocket (Fig. 10D). Astragaloside IV formed two hydrogen bonds, primarily engaging the backbone of Gly331, complemented by extensive hydrophobic contacts owing to its larger size (Fig. 10E). Astragaloside VII formed hydrogen bonds with the side chain of Arg305 and the backbone of Gly331, while also participating in hydrophobic interactions (Fig. 10F). In contrast, senkyunolide H, consistent with its unbound state, did not form persistent hydrogen bonds within the canonical ATP-binding site in its most populated cluster, interacting transiently and non-specifically with the protein surface (Fig. 10G). Overall, the simulations highlighted considerable differences in binding stability among the ligands within the PDK4 ATP-binding site, correlating with their specific interaction modes. Notably, astragaloside IV and VII achieved greater stability through hydrogen bonds with key residues like Gly331 and Arg305 and extensive hydrophobic contacts, whereas apigenin formed fewer persistent interactions, and senkyunolide H remained largely unbound owing to a lack of specific stabilizing contacts within the site.

3.9. Senkyunolide H and apigenin are active YXS components regulating energy metabolism

To further investigate the mechanism of action of individual YXS components, we measured cell viability and PDH enzyme activity following treatment with the PDK4 inhibitor DCA or the FOXO1 inhibitor AS1842856 (Figs. 11A–11D). In the presence of these inhibitors, senkyunolide H, apigenin, astragaloside IV, and astragaloside VII significantly enhanced cell viability and PDH en-

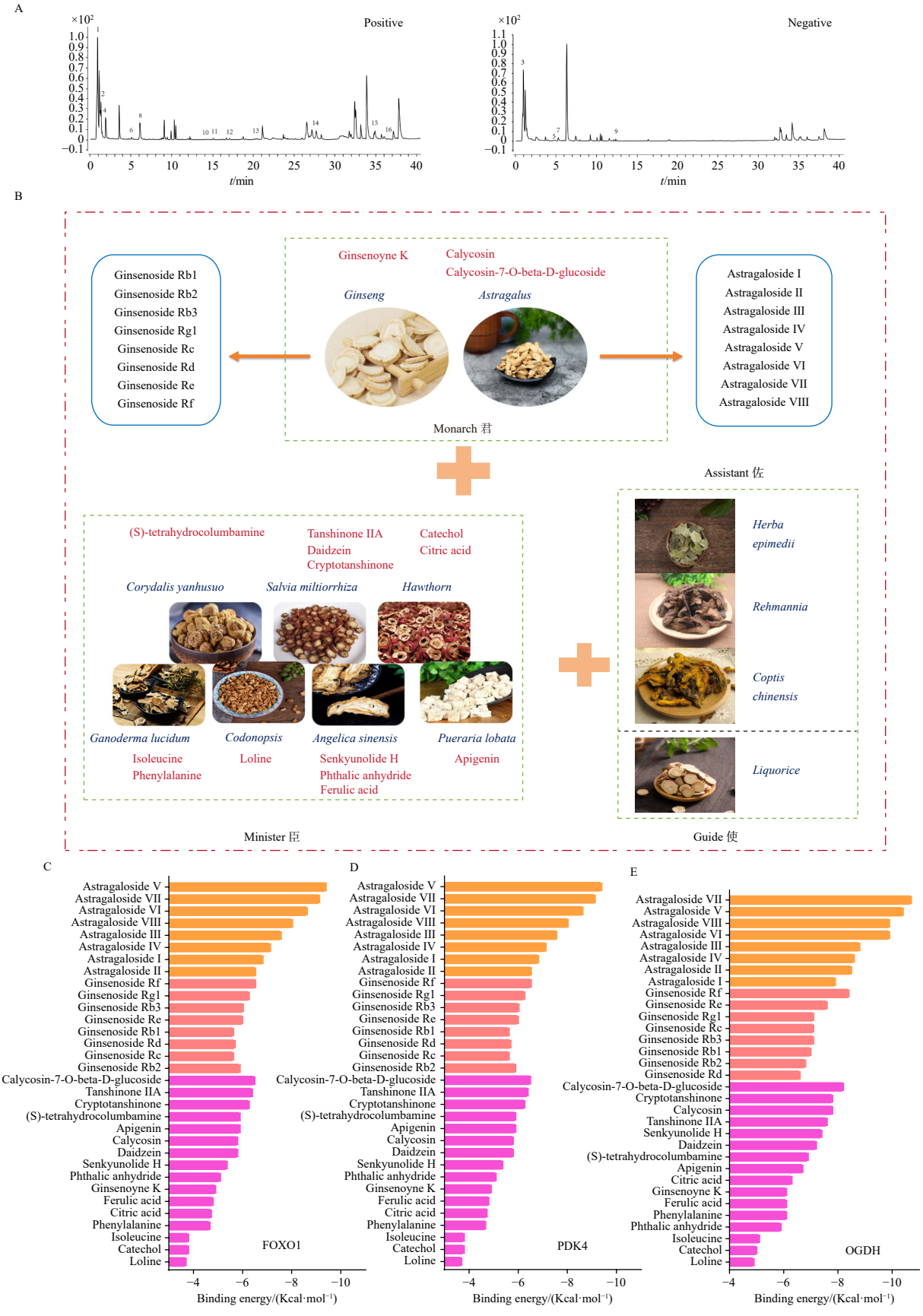

Fig. 8 Molecular docking analysis of YXS components with FOXO1, PDK4, and OGDH. (A) TICs recorded in positive and negative ion modes. (B) Sixteen blood components and 16 principal saponins from ginseng and Astragalus selected for subsequent investigation. (C-E) Molecular docking analysis of all 32 compounds with FOXO1, PDK4, and OGDH, respectively. OGDH, oxoglutarate dehydrogenase; YXS, Yangxinshi Tablet.

zyme activity, both of which are closely related to energy metabolism. Using H9c2 cells, mitochondrial respiration and energy metabolism were assessed with the Agilent Seahorse XFp Cell Mito Stress Test to elucidate the mechanisms underlying the pro-

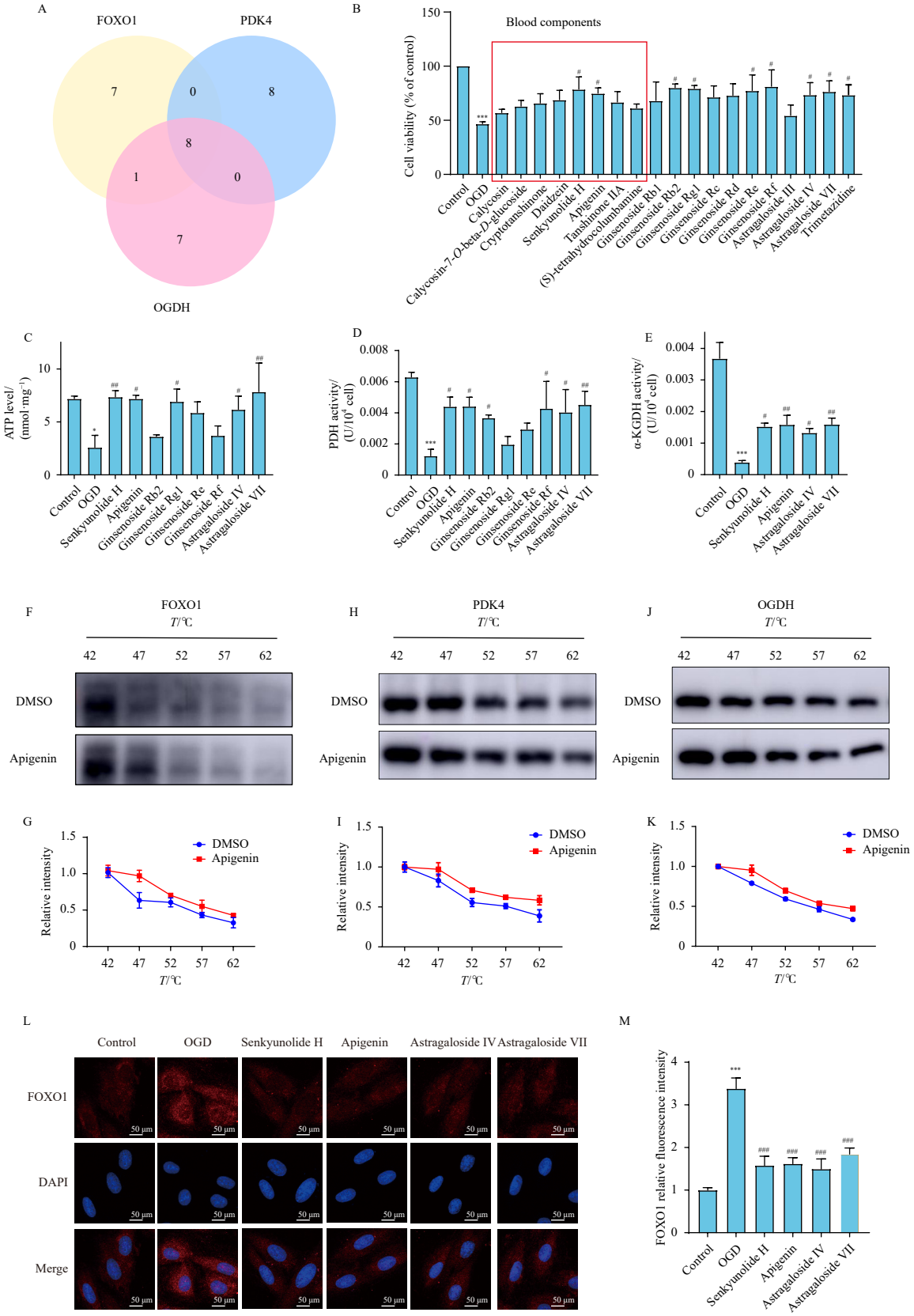

Fig. 9 FOXO1 is a target of key YXS compounds. (A) Schematic diagram showing the overlap among the 16 blood components. (B–E) Cell viability, ATP levels, and PDH and α-KGDH activities in H9c2 cells pretreated with various compounds (10 μmol·L^{-1} for 24 h) followed by exposure to OGD conditions. (F–K) Effects of apigenin on the thermal stability of FOXO1, PDK4, and OGDH analyzed by cellular thermal shift assay. (L–M) Immunofluorescence analysis of FOXO1 expression in H9c2 cells treated with the compounds. Scale bar = 50 μm. Data are analyzed using one-way ANOVA with LSD post-hoc test after confirmation of homogeneity of variance. Data are expressed as mean ± SEM (n = 3). $^{*}P < 0.05$, $^{***}P < 0.001$ *vs* Control group; $^{\#}P < 0.05$, $^{\#\#}P < 0.01$, $^{\#\#\#}P < 0.001$ *vs* OGD group. OGD, oxygen-glucose deprivation; PDH, pyruvate dehydrogenase; YXS, Yangxinshi Tablet.

tective effects of the active compounds. Treatment of the cells with senkyunolide H and apigenin resulted in varying degrees of improvement in basal respiration, ATP production, and maximal respiration (Figs. 11E–11H). Taken together, senkyunolide H,

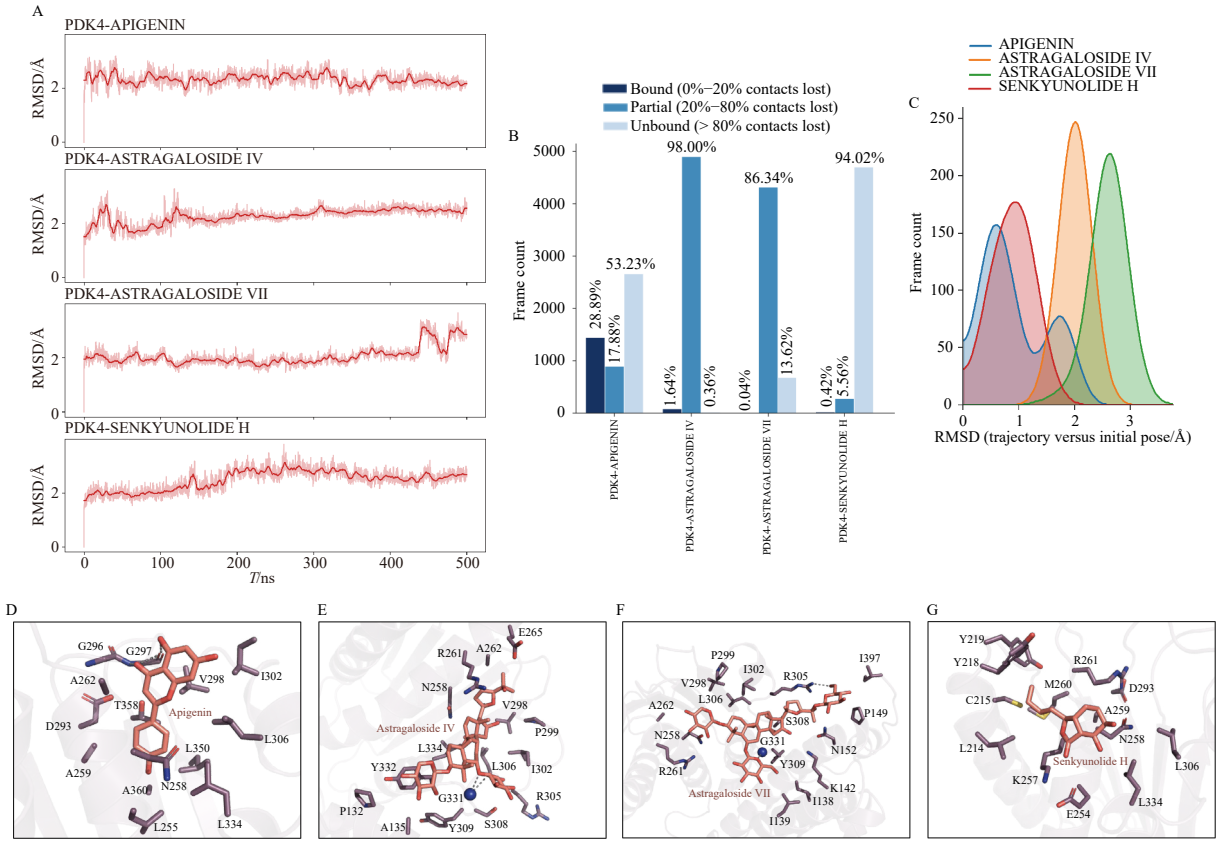

Fig. 10 Molecular dynamics simulation of PDK4 and compounds. (A) Overall structural stability of the protein backbone in each complex. (B) Stability of the ligand binding poses within the ATP-binding site. (C) Ligand mobility. (D–G) Representative structures from the most populated clusters.

apigenin, astragaloside IV, and astragaloside VII were identified as active components of YXS.

Finally, we performed SPR experiments to assess the binding affinity of apigenin to PDK4. We found that apigenin engaged in fast-binding and fast-dissociation kinetics with PDK4, with a K_D value of 8.521×10^{-5} mol·L^{-1}, indicating specific binding to PDK4 (Figs. 11I–11J).

4. Discussion

In the current study, we demonstrated the therapeutic effects and mechanism of action of YXS, a TCM used to treat post-MI HF. *In vivo*, YXS improved cardiac function and exercise endurance, enhanced hemodynamics, reduced inflammatory cell infiltration, and decreased collagen fiber deposition, thereby protecting against post-MI HF. To the best of our knowledge, this is the first study to report that YXS can regulate the TCA cycle and FOXO1/PDK4 signaling to improve metabolism. These findings indicate that YXS prevents post-MI HF by inhibiting FOXO1/PDK4 signaling and enhancing metabolism. Single-cell RNA-seq analysis revealed that cardiomyocytes from patients with HF demonstrated altered energy metabolism. In addition, senkyunolide H, apigenin, astragaloside IV, and astragaloside VII were identified as the main active ingredients of YXS responsible for the observed effects.

HF remains one of the leading causes of cardiovascular disease-associated mortality, with MI being the most common precipitant of HF [47]. Pathophysiological factors contributing to the development of HF during hospitalization for MI include myocardial damage due to necrosis, myocardial dysfunction, and mechanical complications [48]. Despite the implementation of secondary prevention measures, several patients experience adverse left ventricular remodeling, ultimately leading to HF, highlighting the need for further research to mitigate the development and severity of pathophysiological factors and improve patient outcomes [49]. Our study demonstrated the protective effects of YXS against the progression of HF post-MI and elucidated its underlying mechanisms of action in both *in vivo* and *in vitro* models. In rats with post-MI HF, the therapeutic effects of YXS were more pronounced after 4 weeks than after 2 weeks of treatment, as evidenced by the reduced cardiac function in the Mod group, with a marked improvement observed in the YXS group (particularly in the YXS M group). YXS not only improved cardiac function and exercise endurance but also enhanced hemodynamics, reduced inflammatory cell infiltration, and decreased collagen fiber deposition. Additionally, YXS substantially lowered the levels of HF biomarkers, including ANP, BNP, and NT-proBNP. Multiple studies have reported the therapeutic benefits of YXS in rats with chronic ischemic HF by evaluating cardiac function and exercise capacity [28]. Although our findings are consistent with previous reports, we observed that YXS H elicited better exercise endurance than YXS M and YXS L. Our study further determined the protective effects of YXS by assessing HF biomarkers and performing histological staining. Moreover, our study detected hemodynamic indicators for the first time, further highlighting the efficacy of YXS in the treatment of post-MI HF. These findings underscore the notable protective effects of YXS in rats with post-MI HF.

Cardiomyocytes generate substantial amounts of ATP primarily through OXPHOS within the mitochondria [50]. The regulation of the TCA cycle, along with continuous feedback mechanisms involving OXPHOS, is essential for maintaining cellular homeostasis and energy production [51]. During HF, the increased workload on the heart creates an imbalance between energy consumption and energy production from myocardial mitochondria [17]. Hypoxia [52], oxidative stress [53], endoplasmic reticulum stress [54], reactive oxygen species [55], inflammation, and mitochondrial phagocytosis [56] can affect mitochondrial homeostasis, thereby causing damage to cardiac muscle cells [57, 58]. Further-

more, mitochondrial fusion plays a crucial role in the exchange of mtDNA, membrane phospholipids, respiratory-related proteins, and intermediates of the TCA cycle [59, 60]. As the powerhouses of the cell, mitochondria are central regulators of cardiomyocyte homeostasis [60, 61]. Energy demand overload can overwhelm cardiomyocyte mitochondria, affecting their function, a process that is intricately linked to cardiac fibrosis and cardiomyocyte apoptosis. Simultaneously, the transformation of metabolic substrates is accompanied by a reduction in ATP production and an accumulation of LA, ultimately leading to a decline in cardiac function [62]. We conducted an in-depth study on the mechanism of action of YXS and, for the first time, confirmed that YXS improves cardiomyocyte energy homeostasis in post-MI HF by inhibiting FOXO1/PDK4 signaling, regulating OGDH expression in the TCA cycle, and increasing ATP levels to enhance energy metabolism.

The FOXO family of transcription factors is involved in multiple cellular processes, including energy metabolism, redox homeostasis, cell differentiation, and cell cycle arrest [63]. In skeletal muscles, FOXO1 regulates glucose and fatty acid metabolism by down-regulating PDK4 and up-regulating lipoprotein lipase, thereby controlling energy homeostasis [64]. PDK4, the predominant subtype of PDK in the heart, phosphorylates and inactivates PDH, consequently reducing the capacity of cardiomyocytes to oxidize glucose [18, 65]. Accumulating evidence suggests that FOXO1 plays a critical role in cardiometabolic regulation. For instance, in the diabetic myocardium, FOXO1 activation disrupts glycolysis

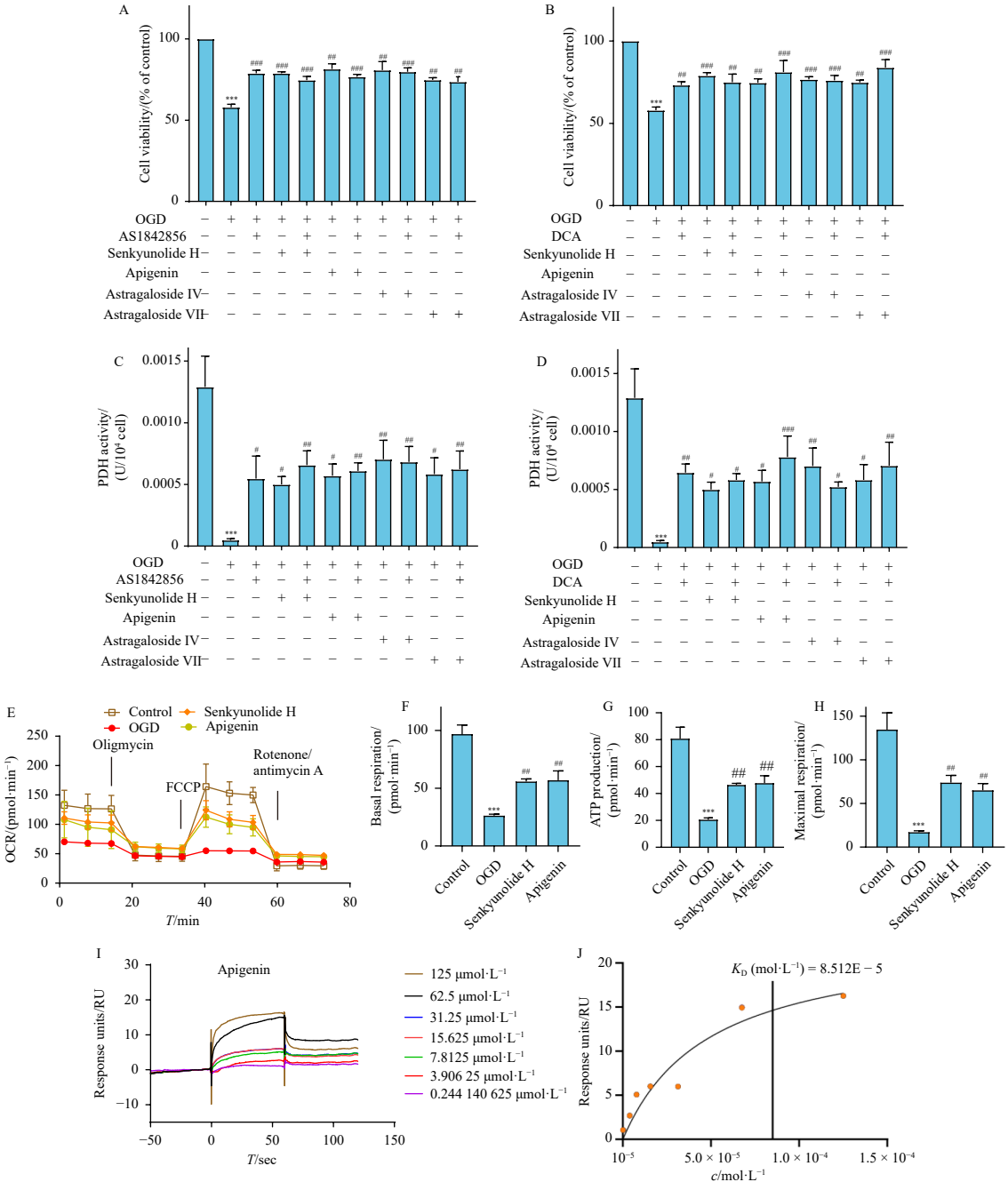

Fig. 11 Senkyunolide H and apigenin are active compounds of YXS that regulate energy metabolism. (A–D) Cell viability and PDH activity were measured in H9c2 cells treated with senkyunolide H, apigenin, astragaloside IV, astragaloside VII, and the FOXO1 and PDK4 inhibitors. (E) Respiration profile of H9c2 cells. OCR is measured in H9c2 cells pretreated with senkyunolide H or apigenin (10 μmol·L^{-1}, 24 h) and then exposed to oxygen-glucose deprivation conditions. (F–H) Quantitative analysis of basal respiration, ATP production, and maximal respiration. (I–J) SPR analysis of apigenin binding to PDK4. Data are analyzed using one-way ANOVA with LSD post-hoc test after confirmation of homogeneity of variance. Data are expressed as mean ± SEM (n = 3). $^{***}P < 0.001$ *vs* Control group; $^{\#}P < 0.05$, $^{\#\#}P < 0.01$, $^{\#\#\#}P < 0.001$ *vs* OGD group. OCR, oxygen consumption rate; YXS, Yangxinshi Tablet.

and glucose oxidation, increases fatty acid oxidation, and elevates PDK4 and CPT1 expression, resulting in mitochondrial and cardiac dysfunction [66]. In addition, nuclear localization of FOXO1 was shown to increase PDK4 expression, leading to lactate accumulation and impaired mitochondrial oxidation, thereby affecting the maintenance of cardiac homeostasis [67]. Building on these previous findings, we observed that YXS enhances mitochondrial respiration *in vitro*. Importantly, our study, for the first time, demonstrates that YXS can inhibit FOXO1/PDK4 signaling, thereby improving cardiomyocyte energy metabolism both *in vivo* and *in vitro*, although this mechanism warrants further in-depth verification. Many studies have extensively explored proteins, examining not only their functional characteristics but also changes at their target sites. Therefore, the effect of YXS on FOXO1/PDK4 could be further investigated by examining changes in its amino acid sites or other structural aspects. To strengthen our findings and provide robust evidence, we conducted single-cell RNA-seq analysis on patients with HF and healthy individuals, revealing a close association between energy metabolism and HF.

Chinese medicines that are absorbed into the blood are considered potential bioactive agents [68, 69]. Numerous studies have reported the active ingredients of YXS. For instance, salvianolic acid B and caffeic acid present in YXS have been identified as potential thrombin inhibitors [70], while salvianolic acids A and B have been shown to possess potent anti-oxidant activities [71]. The efficacy of Ginseng and Astragalus, two key herbal components in formulating YXS, has long been established in the management of cardiovascular diseases. In our study, we analyzed the main active components of YXS and selected the common compounds that ranked among the top 16 in binding energy for each target protein. We focused on ginsenosides and astragaloside saponins as blood-derived components, emphasizing their binding affinity and compound availability for further analysis. Notably, we demonstrated for the first time that senkyunolide H and apigenin are the main active components of YXS responsible for exerting its protective effects and improving energy metabolism. Senkyunolide H, a phthalide compound, possesses multiple pharmacological functions, including neuroprotective effects and the ability to ameliorate oxidative damage, the latter making it useful in cardiovascular diseases [72]. Conversely, apigenin has been shown to improve abnormal glucose and lipid metabolism in H9c2 cells by inhibiting HIF-1α expression, while up-regulating CPT1 and PDK4 expression *via* PPARα signaling and down-regulating PPARγ-mediated expression of GPAT and GLUT4 [73]. Additionally, astragaloside IV and VII, active ingredients of YXS, have been shown to improve energy metabolism. The cardioprotective effects of astragaloside IV could be attributed to the up-regulation of genes and enzymes involved in free fatty acid metabolism, thereby enhancing energy metabolism [74]. Additionally, astragaloside IV alleviates myocardial injury through mitochondrial quality control [75]. Accordingly, astragaloside IV and VII can regulate energy metabolism; however, further research is required to comprehensively clarify their roles in HFrEF after MI.

Nevertheless, our study has some limitations, and further work is needed to fully elucidate the key active compounds of YXS. Based on previous efficacy studies, we not only incorporated hemodynamic assessments but also performed a more in-depth investigation of the underlying mechanisms of YXS and its compounds both *in vivo* and *in vitro*. The binding sites of YXS with its targets are not sufficiently clear, the investigation of active substances is not in-depth enough, and the research on YXS regarding mitochondrial function and structure is not well-defined. It is recommended that more comprehensive studies be conducted in the future.

In summary, this is the first study to demonstrate that YXS can improve energy metabolism by inhibiting FOXO1/PDK4 signaling in post-MI HF. Furthermore, senkyunolide H, apigenin, astragaloside IV, and astragaloside VII exhibited notable protective effects against OGD-induced damage in H9c2 cells and were identified as the main active ingredients of YXS (Fig. 12). This study elucidates a new mechanism through which YXS exerts its protective effects, clarifying the active substance basis of YXS. It fur-

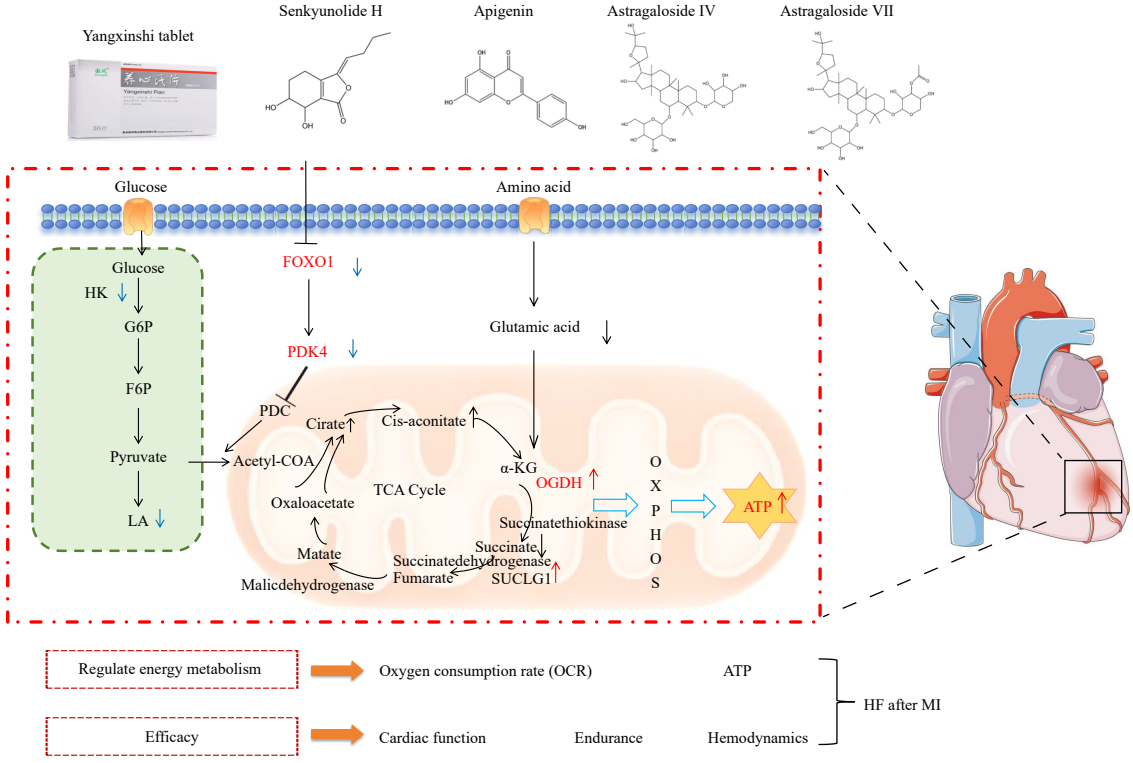

Fig. 12 Schematic diagram illustrating the mechanism of action of YXS in heart failure. YXS improves energy metabolism by inhibiting FOXO1/PDK4 signaling and regulating the TCA cycle and ATP levels in rats with post-myocardial infarction heart failure. Senkyunolide H, apigenin, astragaloside IV, and astragaloside VII are identified as the active ingredients of YXS in H9c2 cells under oxygen-glucose deprivation conditions. TCA, tricarboxylic acid; YXS, Yangxinshi Tablet.

ther provides insights for the study of TCM formulas and lays a foundation for the clinical research of YXS. In the future, we may also integrate TCM with Western medicine to conduct joint pharmacological studies.

5. Conclusion

Our study demonstrates that YXS can inhibit FOXO1/PDK4 signaling to improve energy metabolism. Moreover, our single-cell RNA-seq analysis revealed a close association between HF and energy metabolism. Additionally, we applied a novel approach to screen for active compounds in YXS. Furthermore, we identified senkyunolide H, apigenin, astragaloside IV, and astragaloside VII as the primary active ingredients of YXS responsible for its cardioprotective effects. Our study comprehensively demonstrates the mechanism by which YXS improves the energy requirements of cardiomyocytes in post-MI HF and further validates the clinical application of YXS in treating HF.

Funding

This work was supported by the National Program for NSFC, China (No. 82474310), and the Innovation Team and Talents Cultivation Program of the National Administration of Traditional Chinese Medicine (No. ZYYCXTD-C-202203).

Declaration of competing interests

These authors have no conflict of interest to declare

References

1 Savarese G, Stolfo D, Sinagra G, et al. Heart failure with mid-range or mildly reduced ejection fraction. *Nat Rev Cardiol*. 2022;19(2):100-116. https://doi.org/10.1038/s41569-021-00605-5.
2 Murphy SP, Ibrahim NE, Januzzi JL Jr. Heart failure with reduced ejection fraction: a review. *JAMA*. 2020;324(5):488-504. https://doi.org/10.1001/jama.2020.10262.
3 Yurista SR, Eder RA, Welsh A, et al. Ketone ester supplementation suppresses cardiac inflammation and improves cardiac energetics in a swine model of acute myocardial infarction. *Metabolism*. 2023;145:155608. https://doi.org/10.1016/j.metabol.2023.155608.
4 Zhu T, Chen J, Zhang MX, et al. Tanshinone IIA exerts cardioprotective effects through improving gut-brain axis post-myocardial infarction. *Cardiovasc Toxicol*. 2024;24(12):1317-1334. https://doi.org/10.1007/s12012-024-09928-4.
5 Heidenreich PA, Bozkurt B, Aguilar D, et al. 2022 AHA/ACC/HFSA guideline for the management of heart failure: executive summary: a report of the American College of Cardiology/American Heart Association Joint Committee on clinical practice guidelines. *J Am Coll Cardiol*. 2022;79(17):1757-1780. https://doi.org/10.1016/j.jacc.2021.12.011.
6 Frantz S, Hundertmark MJ, Schulz-Menger J, et al. Left ventricular remodelling post-myocardial infarction: pathophysiology, imaging, and novel therapies. *Eur Heart J*. 2022;43(27):2549-2561. https://doi.org/10.1093/eurheartj/ehac223.
7 Del Buono MG, Moroni F, Montone RA, et al. Ischemic cardiomyopathy and heart failure after acute myocardial infarction. *Curr Cardiol Rep*. 2022;24(10):1505-1515. https://doi.org/10.1007/s11886-022-01766-6.
8 Agostini LDC, Silva NNT, Belo VA, et al. Pharmacogenetics of angiotensin-converting enzyme inhibitors (ACEI) and angiotensin II receptor blockers (ARB) in cardiovascular diseases. *Eur J Pharmacol*. 2024;981:176907. https://doi.org/10.1016/j.ejphar.2024.176907.
9 Rossi GP, Rossi FB, Guarnieri C, et al. Clinical management of primary aldosteronism: an update. *Hypertension*. 2024;81(9):1845-1856. https://doi.org/10.1161/HYPERTENSIONAHA.124.22642.
10 Packer M, McMurray JJV. Importance of endogenous compensatory vasoactive peptides in broadening the effects of inhibitors of the renin-angiotensin system for the treatment of heart failure. *Lancet*. 2017;389(10081):1831-1840. https://doi.org/10.1016/S0140-6736(16)30969-2.
11 Capone F, Sotomayor-Flores C, Bode D, et al. Cardiac metabolism in HFpEF: from fuel to signalling. *Cardiovasc Res*. 2023;118(18):3556-3575. https://doi.org/10.1093/cvr/cvac166.
12 Murashige D, Jang C, Neinast M, et al. Comprehensive quantification of fuel use by the failing and nonfailing human heart. *Science*. 2020;370(6514):364-368. https://doi.org/10.1126/science.abc8861.
13 Chen J, Wei X, Zhang Q, et al. The traditional Chinese medicines treat chronic heart failure and their main bioactive constituents and mechanisms. *Acta Pharm Sin B*. 2023;13(5):1919-1955. https://doi.org/10.1016/j.apsb.2023.02.005.
14 Takada S, Maekawa S, Furihata T, et al. Succinyl-CoA-based energy metabolism dysfunction in chronic heart failure. *Proc Natl Acad Sci U S A*. 2022;119(41):e2203628119. https://doi.org/10.1073/pnas.2203628119.
15 Lopaschuk GD, Karwi QG, Tian R, et al. Cardiac energy metabolism in heart failure. *Circ Res*. 2021;128(10):1487-1513. https://doi.org/10.1161/CIRCRESAHA.121.318241.
16 Ha CM, Wende AR. Abstract MP204: pyruvate dehydrogenase kinase isozyme specific regulation of protein acetylation in cardiac tissue. *Circ Res*. 2021;129(Suppl_1):AMP204. https://doi.org/10.1161/res.129.suppl_1.MP204.
17 Murphy MP, Hartley RC. Mitochondria as a therapeutic target for common pathologies. *Nat Rev Drug Discov*. 2018;17(12):865-886. https://doi.org/10.1038/nrd.2018.174.
18 Ioannilli L, Ciccarone F, Ciriolo MR. Adipose tissue and FoxO1: bridging physiology and mechanisms. *Cells*. 2020;9(4):849. https://doi.org/10.3390/cells9040849 .
19 Gopal K, Saleme B, Al Batran R, et al. FoxO1 regulates myocardial glucose oxidation rates *via* transcriptional control of pyruvate dehydrogenase kinase 4 expression. *Am J Physiol Heart Circ Physiol*. 2017;313(3):H479-H490. https://doi.org/10.1152/ajpheart.00191.2017.
20 Gao K, Zhang J, Gao P, et al. Qishen granules exerts cardioprotective effects on rats with heart failure *via* regulating fatty acid and glucose metabolism. *Chin Med*. 2020;15:21. https://doi.org/10.1186/s13020-020-0299-9.
21 Sun Q, Karwi QG, Wong N, et al. Advances in myocardial energy metabolism: metabolic remodeling in heart failure and beyond. *Cardiovasc Res*. 2024;120(16):1996-2016.https://doi.org/10.1093/cvr/cvae231 .
22 Layne K, Ferro A. Traditional Chinese medicines in the management of cardiovascular diseases: a comprehensive systematic review. *Br J Clin Pharmacol*. 2017;83(1):20-32. https://doi.org/10.1111/bcp.13013.
23 Wang J, Lu LH, Wang Y, et al. Qishenyiqi Dropping Pill attenuates myocardial fibrosis in rats by inhibiting RAAS-mediated arachidonic acid inflammation. *J Ethnopharmacol*. 2015;176:375-384. https://doi.org/10.1016/j.jep.2015.11.023.
24 Wang J, Zhou J, Wang Y, et al. Qiliqiangxin protects against anoxic injury in cardiac microvascular endothelial cells *via* NRG-1/ErbB-PI3K/Akt/mTOR pathway. *J Cell Mol Med*. 2017;21(9):1905-1914. https://doi.org/10.1111/jcmm.13111.
25 Lu SH, Yu YF, Dai SS, et al. Efficacy and safety of Yangxinshi Tablet for chronic heart failure: a systematic review and meta-analysis. *World J Clin Cases*. 2024;12(13):2218-2230. https://doi.org/10.12998/wjcc.v12.i13.2218.
26 Li Y, Li Y, Zhang ZJ, et al. Efficacy and safety of yangxinshi versus trimetazidine on exercise tolerance in patients with coronary heart disease after percutaneous coronary intervention: multicenter, double-blind clinical trial. *Phytomedicine*. 2024;135:156198. https://doi.org/10.1016/j.phymed.2024.156198.
27 Zhang S, Shen Y, Liu P, et al. Yangxinshi Tablet improves exercise capacity for patients with coronary heart disease: results from a randomized, double-blind, placebo-controlled, and multicenter trial. *Rev Cardiovasc Med*. 2022;23(8):266. https://doi.org/10.31083/j.rcm2308266.
28 Wu RM, Jiang B, Li H, et al. A network pharmacology approach to discover action mechanisms of Yangxinshi Tablet for improving energy metabolism in chronic ischemic heart failure. *J Ethnopharmacol*. 2020;246:112227. https://doi.org/10.1016/j.jep.2019.112227.
29 Song H, Liu C, Yang Z, et al. Yangxinshi Tablet protects against myocardial injury and increases skeletal muscle exercise capacity by regulating mitochondrial bioenergetics. *Phytomedicine*. 2025;145:156990. https://doi.org/10.1016/j.phymed.2025.156990.
30 Chen L, Cao Y, Zhang H, et al. Network pharmacology-based strategy for predicting active ingredients and potential targets of Yangxinshi Tablet for treating heart failure. *J Ethnopharmacol*. 2018;219:359-368. https://doi.org/10.1016/j.jep.2017.12.011.
31 Zhou Z, Li M, Zhang Z, et al. Overview of *Panax ginseng* and its active ingredients protective mechanism on cardiovascular diseases. *J Ethnopharmacol*. 2024;334:118506. https://doi.org/10.1016/j.jep.2024.118506.
32 Liu Y, Xu W, Xiong Y, et al. Evaluations of the effect of HuangQi against heart failure based on comprehensive echocardiography index and metabonomics. *Phytomedicine*. 2018;50:205-212. https://doi.org/10.1016/j.phymed.2018.04.027.
33 Zang Y, Wan J, Zhang Z, et al. An updated role of astragaloside IV in heart failure. *Biomed Pharmacother*. 2020;126:110012. https://doi.org/10.1016/j.biopha.2020.110012.
34 Chen R, Meng K, Wang C, et al. Effects of Tongmai Yangxin Pills on ventricular remodeling in myocardial ischemia-reperfusion rats. *Acupunct Herbal Med*. 2023;3(2):126-136. https://doi.org/10.1097/HM9.0000000000000024.
35 Luo B, Wang W, Li Y, et al. Tetramethylpyrazine attenuates chronic intermittent hypoxia-exacerbated diabetic atherosclerosis: a mechanistic study of the IRE1α-XBP1 signaling pathway. *Acupunct Herbal Med*. 2025;5(2):160-172. https://doi.org/10.1097/HM9.0000000000000154.
36 Huang Y, Zhang K, Wang X, et al. Multi-omics approach for identification of molecular alterations of QiShenYiQi Dripping Pills in heart failure with preserved ejection fraction. *J Ethnopharmacol*. 2023;315:116673. https://doi.org/10.1016/j.jep.2023.116673.
37 Koenig AL, Shchukina I, Amrute J, et al. Single-cell transcriptomics reveals cell-type-specific diversification in human heart failure. *Nat Cardiovasc Res*. 2022;1(3):263-280. https://doi.org/10.1038/s44161-022-00028-6.
38 Fang J, Li R, Zhang Y, et al. Aristolone in *Nardostachys jatamansi* DC. induces mesenteric vasodilation and ameliorates hypertension *via* activation of the K(ATP) channel and PDK1-Akt-eNOS pathway. *Phytomedicine*. 2022;104:154257. https://doi.org/10.1016/j.phymed.2022.154257.
39 Wada Y, Kidokoro K, Kondo M, et al. Evaluation of glomerular hemodynamic changes by sodium-glucose-transporter 2 inhibition in type 2 diabetic rats

using *in vivo* imaging. *Kidney Int*. 2024;106(3):408-418. https://doi.org/10.1016/j.kint.2024.05.006 .
40 Anderson NM, Mucka P, Kern JG, et al. The emerging role and targetability of the TCA cycle in cancer metabolism. *Protein Cell*. 2018;9(2):216-237. https://doi.org/10.1007/s13238-017-0451-1.
41 Gross DN, Wan M, Birnbaum MJ. The role of FOXO in the regulation of metabolism. *Curr Diab Rep*. 2009;9(3):208-214. https://doi.org/10.1007/s11892-009-0034-5.
42 Zhu X, Wang Y, Soaita I, et al. Acetate controls endothelial-to-mesenchymal transition. *Cell Metab*. 2023;35(7):1163-1178.e10. https://doi.org/10.1016/j.cmet.2023.05.010.
43 Liehr T, Kankel S, Hardt KS, et al. Genetic and molecular characterization of H9*c*2 rat myoblast cell line. *Cells*. 2025;14(7):502.https://doi.org/10.3390/cells14070502 .
44 Li J, Chen X, Liu R, et al. Engineering novel scaffolds for specific HDAC11 inhibitors against metabolic diseases exploiting deep learning, virtual screening, and molecular dynamics simulations. *Int J Biol Macromol*. 2024;262(Pt 2):129810. https://doi.org/10.1016/j.ijbiomac.2024.129810 .
45 Zhu W, He Y. α-Ketoglutarate dehydrogenase (KGDH): a new balancer between energy metabolism and gene expression in plants. *J Integr Plant Biol*. 2023;65(8):1843-1845. https://doi.org/10.1111/jipb.13544 .
46 Wynn RM, Kato M, Chuang JL, et al. Pyruvate dehydrogenase kinase-4 structures reveal a metastable open conformation fostering robust core-free basal activity. *J Biol Chem*. 2008;283(37):25305-25315. https://doi.org/10.1074/jbc.M802249200.
47 Roger VL. Epidemiology of heart failure. *Circ Res*. 2013;113(6):646-659. https://doi.org/10.1161/CIRCRESAHA.113.300268.
48 Jenca D, Melenovsky V, Stehlik J, et al. Heart failure after myocardial infarction: incidence and predictors. *ESC Heart Fail*. 2021;8(1):222-237. https://doi.org/10.1002/ehf2.13144.
49 Westman PC, Lipinski MJ, Luger D, et al. Inflammation as a driver of adverse left ventricular remodeling after acute myocardial infarction. *J Am Coll Cardiol*. 2016;67(17):2050-2060. https://doi.org/10.1016/j.jacc.2016.01.073.
50 Nolfi-Donegan D, Braganza A, Shiva S. Mitochondrial electron transport chain: oxidative phosphorylation, oxidant production, and methods of measurement. *Redox Biol*. 2020;37:101674. https://doi.org/10.1016/j.redox.2020.101674.
51 Martinez-Reyes I, Chandel NS. Mitochondrial TCA cycle metabolites control physiology and disease. *Nat Commun*. 2020;11(1):102. https://doi.org/10.1038/s41467-019-13668-3.
52 Chang X, Zhou S, Huang Y, et al. Zishen Huoxue Decoction (ZSHX) alleviates ischemic myocardial injury (MI) *via* Sirt5-β-tubulin mediated synergistic mechanism of "mitophagy-unfolded protein response" and mitophagy. *Chin J Nat Med*. 2025;23(3):311-321. https://doi.org/10.1016/s1875-5364(25)60838-7.
53 Chang X, Zhou SY, Yan ZQ, et al. Potential candidates of natural antioxidants from herbs for treating lung disorders: focus on redox balance and natural products. *Phytother Res*. 2025;39(8):3353-3385. https://doi.org/10.1002/ptr.70008.
54 Yang K, Zhang P, Li JX, et al. Potential of natural drug modulation of endoplasmic reticulum stress in the treatment of myocardial injury. *J Pharm Anal*. 2024;14(11):101034. https://doi.org/10.1016/j.jpha.2024.101034.
55 Pang BX, Dong GT, Pang TL, et al. Emerging insights into the pathogenesis and therapeutic strategies for vascular endothelial injury-associated diseases: focus on mitochondrial dysfunction. *Angiogenesis*. 2024;27(4):623-639. https://doi.org/10.1007/s10456-024-09938-4.
56 Chang X, Zhou H, Hu JL, et al. Targeting mitochondria by lipid-selenium conjugate drug results in malate/fumarate exhaustion and induces mitophagy-mediated necroptosis suppression. *Int J Biol Sci*. 2024;20(14):5793-5811. https://doi.org/10.7150/ijbs.102424.
57 Pu XY, Wu QM, Yan ZQ, et al. The effect of unhealthy lifestyle on the pathogenesis of sick sinus syndrome: a life-guiding review. *Medicine*. 2024;103(43):e39996. https://doi.org/10.1097/MD.0000000000039996.
58 Wu QM, Wang YL, Liu JF, et al. Microtubules and cardiovascular diseases: insights into pathology and therapeutic strategies. *Int J Biochem Cell Biol*. 2024;175:106650. https://doi.org/10.1016/j.biocel.2024.106650.
59 Pu XY, Wu QM, Yan ZQ, et al. Tanshinone IIA modulates Sirt5 and Metll3 interaction to govern mitochondria-endoplasmic reticulum unfolded protein response in coronary microvascular injury. *Phytomedicine*. 2025;145:156982. https://doi.org/10.1016/j.phymed.2025.156982.
60 Wang JY, Zhuang HW, Jia LQ, et al. Nuclear receptor subfamily 4 group A member 1 promotes myocardial ischemia/reperfusion injury through inducing mitochondrial fission factor-mediated mitochondrial fragmentation and inhibiting FUN14 domain containing 1-depedent mitophagy. *Int J Biol Sci*. 2024;20(11):4458-4475. https://doi.org/10.7150/ijbs.95853.
61 Wang JY, Zhuang HW, Li C, et al. Ligustrazine nano-drug delivery system ameliorates doxorubicin-mediated myocardial injury *via* piezo-type mechanosensitive ion channel component 1-prohibitin 2-mediated mitochondrial quality surveillance. *J Nanobiotechnol*. 2025;23(1):383. https://doi.org/10.1186/s12951-025-03420-z.
62 Song R, Dasgupta C, Mulder C, et al. MicroRNA-210 controls mitochondrial metabolism and protects heart function in myocardial infarction. *Circulation*. 2022;145(15):1140-1153. https://doi.org/10.1161/CIRCULATIONAHA.121.056929.
63 Orea-Soufi A, Paik J, Braganca J, et al. FOXO transcription factors as therapeutic targets in human diseases. *Trends Pharmacol Sci*. 2022;43(12):1070-1084. https://doi.org/10.1016/j.tips.2022.09.010.
64 Li Y, Pan H, Zhang X, et al. Geniposide improves glucose homeostasis *via* regulating FoxO1/PDK4 in skeletal muscle. *J Agric Food Chem*. 2019;67(16):4483-4492. https://doi.org/10.1021/acs.jafc.9b00402.
65 Chien HC, Constantin D, Greenhaff PL, et al. PPARα, δ and FOXO1 gene silencing overturns palmitate-induced inhibition of pyruvate oxidation differentially in C2C12 myotubes. *Biology*. 2021;10(11):1098. https://doi.org/10.3390/biology10111098 .
66 Yan D, Cai Y, Luo J, et al. FOXO1 contributes to diabetic cardiomyopathy *via* inducing imbalanced oxidative metabolism in type 1 diabetes. *J Cell Mol Med*. 2020;24(14):7850-7861. https://doi.org/10.1111/jcmm.15418.
67 Khan D, Sarikhani M, Dasgupta S, et al. SIRT6 deacetylase transcriptionally regulates glucose metabolism in heart. *J Cell Physiol*. 2018;233(7):5478-5489. https://doi.org/10.1002/jcp.26434.
68 Li Y, Lin Z, Wang Y, et al. Unraveling the mystery of efficacy in Chinese medicine formula: new approaches and technologies for research on pharmacodynamic substances. *Arab J Chem*. 2022;15(11):104302. https://doi.org/10.1016/j.arabjc.2022.104302.
69 Li Y, Xiang Y, Liang J, et al. The mechanism and treatment strategies of GSDMD-mediated pyroptosis in myocardial infarction. *Acupunct Herbal Med*. 2024;4(3):295-305. https://doi.org/10.1097/HM9.0000000000000129.
70 Liu W, Zhou R, Wen J, et al. Screening thrombin inhibitors from Yangxinshi Tablets by online capillary electrophoresis-based immobilized enzyme microreactor and molecular docking. *Phytochem Anal*. 2025;36(3):520-528. https://doi.org/10.1002/pca.3447 .
71 Zhu J, Yi X, Zhang J, et al. Chemical profiling and antioxidant evaluation of Yangxinshi Tablet by HPLC-ESI-Q-TOF-MS/MS combined with DPPH assay. *J Chromatogr B*. 2017;1060:262-271. https://doi.org/10.1016/j.jchromb.2017.06.022.
72 Jiang Y, Luo Y, Chen X, et al. Senkyunolide H protects PC12 cells from OGD/R-induced injury *via* cAMP-PI3K/AKT signaling pathway. *J Ethnopharmacol*. 2022;282:114659. https://doi.org/10.1016/j.jep.2021.114659.
73 Zhu ZY, Wang F, Jia CH, et al. Apigenin-induced HIF-1α inhibitory effect improves abnormal glucolipid metabolism in Ang Ⅱ /hypoxia-stimulated or HIF-1α-overexpressed H9*c*2 cells. *Phytomedicine*. 2019;62:152713. https://doi.org/10.1016/j.phymed.2018.10.010.
74 Tang B, Zhang JG, Tan HY, et al. Astragaloside IV inhibits ventricular remodeling and improves fatty acid utilization in rats with chronic heart failure. *Biosci Rep*. 2018;38(3):BSR20171036.https://doi.org/10.1042/BSR20171036 .
75 Wang JY, Pu XY, Zhuang HW, et al. Astragaloside IV alleviates septic myocardial injury through DUSP1-Prohibitin 2 mediated mitochondrial quality control and ER-autophagy. *J Adv Res*. 2025;75:561-580. https://doi.org/10.1016/j.jare.2024.10.030.